Energy 324 (2025) 135949

Contents lists available at ScienceDirect

Energy

journal homepage: www.elsevier.com/locate/energy

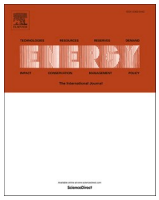

# Benchmarking carbon emissions of coal power against natural gas power via renewable energy integration

Yuhao Shao [a,b], Tian Wu [a,b], Xinrong Yan [c], Chao Yang [a,b,*], Lijie Wang [a,b], Wenxuan Guo [a,b], Yangshu Lin [a,b], Yurong Xie [c], Yi Ding [b,d], Chenghang Zheng [a,b,e,**], Xiang Gao [a,b,e,***]

[a] State Key Lab of Clean Energy Utilization, State Environmental Protection Engineering Center for Coal-Fired Air Pollution Control, Zhejiang University, Hangzhou, 310027, China
[b] Institute of Carbon Neutrality, Zhejiang University, Hangzhou, 310027, China
[c] Huadian Electric Power Research Institute Co., LTD., Hangzhou, 310030, China
[d] College of Electrical Engineering, Zhejiang University, Hangzhou, 310027, China
[e] Zhejiang Baima Lake Laboratory Co., Ltd., Hangzhou, 310051, China

ARTICLE INFO

Handling editor: Isabel Soares

ABSTRACT

This study develops an integrated power system combining coal-fired power plants (CFPP) with photovoltaic, wind power, and hybrid energy storage systems, with particular focus on revealing operational characteristics to inform practical system management. Through assessment of system economics and detailed analysis of seasonal and daily operation characteristics, this study reveals four key findings: (1) The integrated system achieves a 12 % reduction in levelized cost of electricity (0.563 vs. 0.643 CNY/kWh) while maintaining specific $CO_2$ emission comparable to natural gas power (349g $CO_2$/kWh); (2) Specific $CO_2$ emission exhibit distinct temporal patterns, reaching minimum levels during summer daylight hours (10:00–18:00), primarily influenced by renewable resource availability and power demand fluctuations; (3) The proposed optimized CFPP operation strategy featuring lower load during daytime and higher load during nighttime demonstrates effective peak-shaving capability and improved system reliability during peak consumption periods; (4) Battery energy storage system primarily handles daily peak-shaving with predictable operation characteristics conducive to battery health maintenance, while the thermal energy storage system effectively compensates for renewable energy fluctuations and power demand variability. These findings highlight potential pathways for integrated system optimization, suggesting that future efforts could focus on time-dependent emission control strategies, enhanced flexibility in coal plant operation, and storage system management approaches considering equipment health implications. The results demonstrate how operational characteristics analysis can reveal synergies in conventional-renewable hybrid systems.

Nomenclature

| Abbreviation and Subscript | Full Term |
|---|---|
| BESS | Battery energy storage system |
| CFPP | Coal-fired power plant |
| ch | charge |
| dch | discharge |
| GHI | global horizontal irradiance |

(continued on next column)

(continued)

(continued on next page)

* Corresponding author. State Key Lab of Clean Energy Utilization, State Environmental Protection Engineering Center for Coal-Fired Air Pollution Control, Zhejiang University, Hangzhou, 310027, China.
** Corresponding author. State Key Lab of Clean Energy Utilization, State Environmental Protection Engineering Center for Coal-Fired Air Pollution Control, Zhejiang University, Hangzhou, 310027, China.
*** Corresponding author. State Key Lab of Clean Energy Utilization, State Environmental Protection Engineering Center for Coal-Fired Air Pollution Control, Zhejiang University, Hangzhou, 310027, China.
*E-mail addresses:* ychao@zju.edu.cn (C. Yang), zhengch2003@zju.edu.cn (C. Zheng), xgao1@zju.edu.cn (X. Gao).

https://doi.org/10.1016/j.energy.2025.135949
Received 15 October 2024; Received in revised form 12 February 2025; Accepted 31 March 2025
Available online 3 April 2025

(*continued*)

| Abbreviation and Subscript | Full Term |
|---|---|
| NOCT | normal operation cell temperature |
| PCS | Power conversion system |
| PV | Photovoltaic system |
| STC | Standard test condition |
| TESS | Thermal energy storage system |
| WT | Wind turbine |

| Symbol | Definition | Unit |
|---|---|---|
| $\alpha$ | Specific $CO_2$ emission | g $CO_2$/kWh |
| $\beta_{CFPP}$ | Standard coal consumption for power supply of CFPP | g/kWh |
| $\eta$ | Efficiency | % |
| $\theta_{coal}$ | $CO_2$ emission factor of coal | kg $CO_2$/kg |
| $\gamma_{minimum}$ | Minimum load rate of CFPP | % |
| $\gamma_{ramp}$ | Ramp rate of CFPP | %/min |
| $\sigma_{cof}$ | Temperature coefficient of PV cell | %/°C |
| Cap | Installed capacity | MW (MWh) |
| GHI | Global horizontal irradiance | W/$m^2$ |
| h | hub height | m |
| I | Investment cost | CNY |
| k | Annual fixed O&M cost ratio | % |
| LCOE | Levelized cost of electricity | CNY/kWh |
| $m_{coal}$ | Annual mass consumption of coal | kg |
| OM | Annual fixed operation and maintenance cost | CNY |
| P | Power | MW |
| $p_{coal}$ | price of coal | CNY/t |
| $q_{coal}$ | Heat value of coal | kJ/kg |
| r | Discount rate | % |
| t | Time | h |
| T | Temperature | °C |
| UI | Unit investment cost | CNY/kW (CNY/kWh) |
| v | Wind speed | m/s |
| V | Annual variable operation cost | CNY |

## 1. Introduction

### 1.1. Motivation

The Paris Agreement has set an international objective to confront climate change, aiming to significantly curb the global average surface temperature rise to less than 2 °C above pre-industrial levels, with an ambitious target of striving for a limit of merely 1.5 °C increase [1]. The decarbonization of energy combustion processes emerges as a pivotal aspect, with numerous scholars advocating for the exploration of decarbonization pathways [2,3]. These pathways are essential for modeling energy transformations and informing climate policy analyses.

Currently, the energy sector endeavors to reduce $CO_2$ emissions by accelerating development of renewable energy (RE) technologies [4,5]. However, the intermittent, unpredictable, and random characteristics of RE sources pose challenges to the power system's ability to meet dynamic power demands promptly [6,7]. Despite its high carbon emissions, coal-fired power plants (CFPP), with their exceptional load-following capabilities, serve as an effective way to solve these challenges and remain the primary pathway of power generation in numerous developing nations [8,9]. Therefore, incorporating RE into CFPP is crucial for promoting energy conservation and sustainable development in high energy-consuming industries [10].

### 1.2. Literature review

Several scholars have constructed systems that demonstrate various approaches to integrating RE and CFPP. Specifically, solar energy can be directly incorporated into CFPP, thereby enhancing operational efficiency and mitigating emissions [11]. Alternatively, solar energy can be utilized to preheat feedwater or generate steam, leading to a reduction in coal consumption [12]. Besides, the surplus energy produced by renewable sources that is not immediately consumed is capable of being preserved in energy storage systems, ensuring its availability for future use [13,14].

A case study conducted in northeast China evaluated the performance of a wind power and thermal power integrated system with different wind power penetration levels [15]. This investigation revealed that thermal power plants with deep peak regulation capabilities were more effective in handling wind power fluctuations, thereby enhancing the efficiency of the integrated system. Using EnergyPLAN [16], a model of China's integrated energy system for 2020 was constructed, which incorporated components such as heat pumps and thermal storage systems. The simulation results highlighted substantial improvements in the utilization of renewable energy sources, accompanied by notable reductions in annual operational costs and fuel consumption. Liu et al. [17] employed the non-dominated sorting genetic algorithm to conduct a multi-objective optimization of a power plant, incorporating diverse configurations of photovoltaic (PV) systems, concentrated solar power (CSP), battery energy storage systems (BESS), thermal energy storage systems (TESS). Yang et al. [18] highlighted the economic benefits of incorporating batteries into a hybrid renewable energy system, emphasizing their role in significantly reducing the loss of power supply probability (LPSP), especially when the investment costs for PV plants, batteries, and inverters are relatively low. Li et al. [19] introduced a two-stage stochastic optimization framework for optimizing the capacity of hybrid renewable energy systems. They devised a method that integrates an enhanced differential evolution algorithm with the Cplex solver, and successfully validated the effectiveness of this method through a case study. The literature overviews of multi-energy integrated systems are summarized in Table 1.

Research on multi-energy integrated systems demonstrated the system's capability to integrate better energy consumption patterns and optimize overall energy costs [20]. However, the following problems remain.

- The absence of a comprehensive evaluation for multi-energy integrated systems. This oversight prevents a deep understanding of the system's positive and negative aspects, as the analysis usually culminates in levelized cost of energy (LCOE) and similar evaluation metrics. The multi-energy integrated systems encompass diverse characteristics, which are challenging to quantify and significantly influence their practical value.

**Table 1**
Literature overviews of evaluation metrics and methods of multi-energy integrated systems.

| References | Systems | Evaluation metrics | Methods |
|---|---|---|---|
| [11] | CSP + CFPP | Thermal-to-electricity conversion efficiency, ramp rate et al. | Parameter identification and simulation |
| [12] | CSP + CFPP | Payback period, $CO_2$ emission reduction, thermo-economic generation cost et al. | Thermo-economic evaluation |
| [15] | PV + WT + CFPP | Power loss, composite score of the subsystem et al. | Two-stage stochastic optimization |
| [16] | PV + WT + CHP + BESS + TESS | $CO_2$ emission, annual cost, fuel consumption et al. | Modelling and simulation |
| [17] | PV + CSP + BESS + TESS | Levelized cost of energy, loss of power supply probability | Multi-objective optimization (non-dominated sorting genetic algorithm) |
| [18] | PV + WT + CSP + BESS + TESS | Levelized cost of energy, loss of power supply probability | Non-dominated Sorting Genetic Algorithm |
| [19] | WT + CSP + TESS | Levelized cost of energy, loss of power supply probability | Improved differential evolution algorithm |

- Lack of comprehensive analysis of the operating characteristics of each sub-system. Seasonal variations directly influence renewable energy resources, subsequently impacting the output of renewable power plants. Therefore, it is crucial to obtain the seasonal variability in the operational patterns of each sub-system to guide policy implementation effectively.

### 1.3. Contributions

This study addresses critical gaps in existing research by focusing on the CFPP-RE integrated low-carbon power system, presenting three key innovations.

- An optimal system design has been developed through configuration optimization methods, benchmarking carbon emissions against natural gas combined cycle (NGCC) plants. This design reduces the levelized cost of electricity by 12 %, meeting the critical need for cost-effective low-carbon solutions.
- A novel methodology for analyzing temporal operation characteristics has been introduced, revealing previously unrecognized seasonal and daily variations in $CO_2$ emissions, CFPP load rates, and the state of charge (SOC) of energy storage systems. This analytical framework provides valuable insights for optimizing operations in integrated power systems.
- An innovative operational strategy has been developed to effectively utilize the load-following capabilities of CFPP, demonstrating how conventional power plants can be retrofitted to support renewable energy integration, while ensuring system reliability and operational flexibility.

These innovations collectively provide comprehensive technical solutions and operational insights for the transition to low-carbon power system, representing contributions in addressing the challenges of renewable energy integration and power system decarbonization.

## 2. System description

Fig. 1 illustrates the CFPP-based integrated low-carbon power system, which is composed of four sub-systems. The upper sub-system represents the coal-fired power plant (CFPP), where coal is combusted in the boiler to produce heat. The flue gas is treated by the flue gas treatment system before being emitted. The heat generated by boiler is then transferred to the steam-water system and converts feed water into high-temperature steam, which is subsequently sent into steam turbine & generator to produce electricity. The lower sub-system is renewable energy (RE) sub-system, which comprises photovoltaic (PV) and wind turbine (WT) systems, generating electricity from solar and wind energy sources.

The right sub-system is the battery energy storage system (BESS), which is composed of the power conversion system (PCS) and storage block, used for temporarily storing electricity. Specifically, the PCS within BESS serves to convert electricity into a form that can be stored in storage block, which includes AC-DC inverters, DC-DC converters, battery management systems, and other auxiliary devices.

The left sub-system is the thermal energy storage system (TESS), where the electric heater receives power from RE and heats the molten salt. The stored heat in the molten salt tank can subsequently convert feed water into high-temperature steam, which is sent into the steam turbine & generator, producing electricity to compensate for power shortage. The capacity optimization of the TESS configuration considers three parts: the charge part, the discharge part, and the storage part. The charge part includes electric heater, heat exchanger, and pump. The storage part includes the molten salt tank, while the discharge part includes turbine and generator specifically designed for TESS applications. Compared to CFPP, the turbine and generator in TESS require significantly higher operational flexibility to accommodate intermittent operation patterns dictated by stored energy. This flexibility requirement results in a higher investment cost compared to conventional turbine and generator. This cost differential has been accounted for in the economic values.

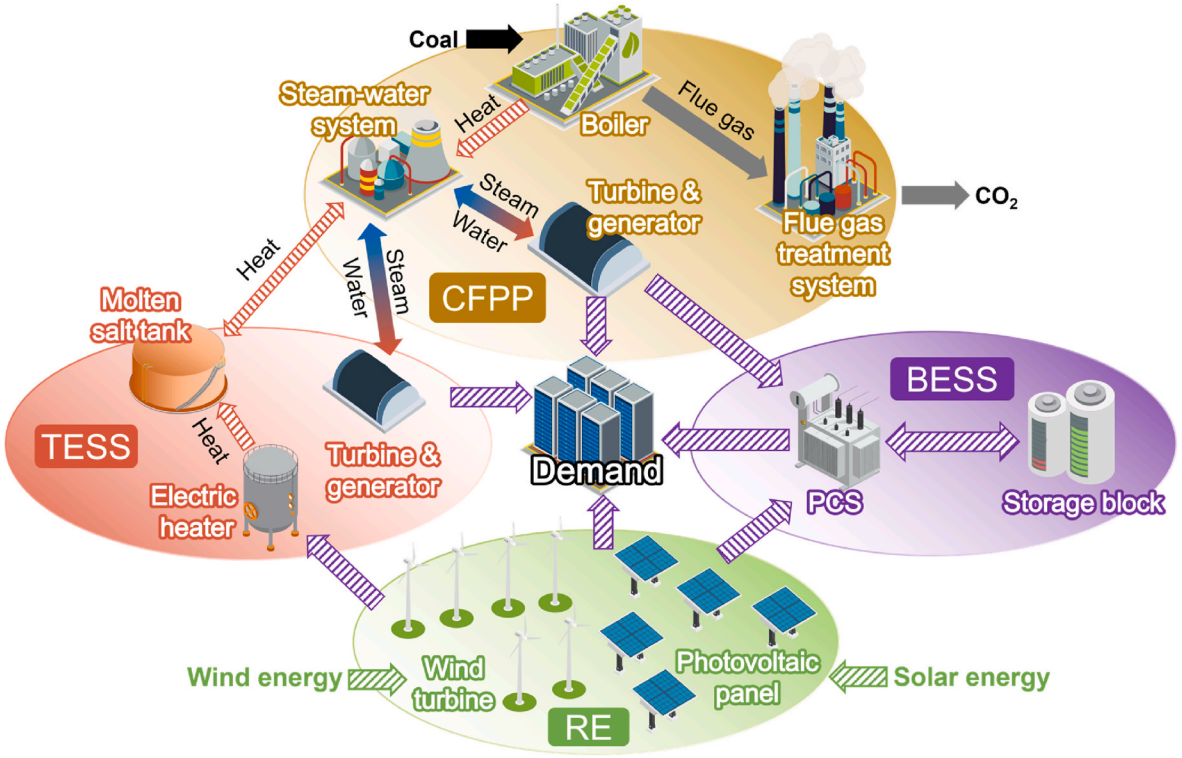


**Fig. 1.** Illustration of the proposed integrated power system.

The four sub-systems work in concert to achieve a balance between meeting power demand with reliability constraints and operating in an economically and low-carbon state.

The natural gas combined cycle (NGCC) power plant is selected as the comparative benchmark based on the following rationales.

(1) NGCC power plants are widely recognized as the cleanest fossil fuel-based power generation technology [21,22]. While producing the same amount of electricity, the $CO_2$ emissions from NGCC are only 46 % of those from CFPP [23,24]. This environmental performance makes NGCC a practical reference for low-carbon system development.
(2) NGCC plants exhibit superior operational flexibility [25,26], characterized by fast ramp rates (up to 15 %/min [27]) and wide operating ranges, enables effective peak-shaving and renewable energy integration, making NGCC a benchmark for assessing the reliability of power systems.

## 3. Methodology

### 3.1. Evaluation and optimization framework

The evaluation and optimization framework of the proposed integrated power system is shown in Fig. 2. Initiating the process, data acquisition encompasses comprehensive parameters such as global horizontal irradiance (GHI), environmental temperature, wind speed, power demand, and techno-economic parameters specific to the research location. Subsequently, the modeling and evaluation step formulate the operation strategy, response priority, and switching logic for the various sub-systems, constituting the simulation module. The simulation module generates operational schedules, providing foundational data for evaluating diverse system configurations. Furthermore, an optimization module is incorporated to identify the optimal configuration.

Within the optimization module, the problem is formulated as a Mixed-Integer Nonlinear Programming (MILP) problem to identify the optimal configuration. The objective of this optimization is to minimize LCOE, subject to two constraints: maintaining power supply reliability above 98 % and ensuring specific $CO_2$ emissions are below 349 g/kWh (NGCC level). The mathematical description of the optimization problem is as follows:

$$\text{Minimize}: \mathrm{LCOE}(\mathbf{X})$$
$$\text{Subject to}: \begin{cases} \text{reliability}(\mathbf{X}) \geq 98\% \\ \alpha(\mathbf{X}) \leq 349\text{g/kWh} \end{cases}$$

where the configuration is denoted as decision variable matrix X, which consists of the installed capacity of CFPP/PV/WT/BESS/TESS. Notably, as detailed in Section 2, the installed capacity of BESS includes both PCS and storage part, while the installed capacity of TESS include charge, discharge and storage part. α is the specific $CO_2$ emission. The detailed computational equations for the three metrics—reliability, specific $CO_2$ emission, and LCOE—are provided in Section 3.2.

The genetic algorithm (GA), renowned for its adaptability in comparable contexts [17,28], has been chosen as the optimization algorithm. Specifically, the population size was set to 300, with the convergence criterion for the optimization defined as: the variations of LCOE must remain below $10^{-10}$ CNY/kWh for at least 50 consecutive generations. Furthermore, even if convergence is achieved, the optimization will continue to run for a minimum of 500 generations. The detailed optimization process is illustrated in Supplementary Fig. 1 of supplementary material.

### 3.2. Operation strategy of the integrated system

The operation strategy of the integrated power system is shown in Fig. 3.

#### 3.2.1. Calculate the power output of RE (PV and WT)

Given the intermittent, unpredictable, and random characteristics of renewable energy sources, the power output of PV and WT should be calculated firstly as Eqs. (1)–(4).

The PV power output $P_{PV}$ is calculated by Eq. (1) [29–31].

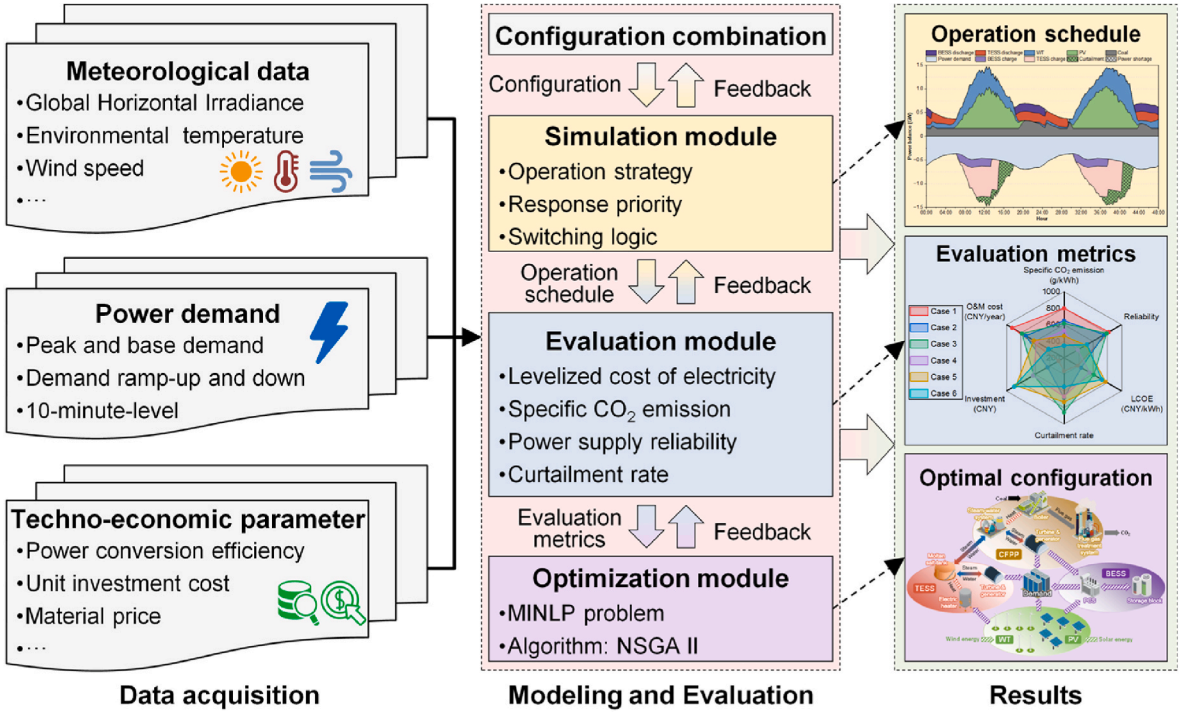


**Fig. 2.** Evaluation and optimization framework of this study.

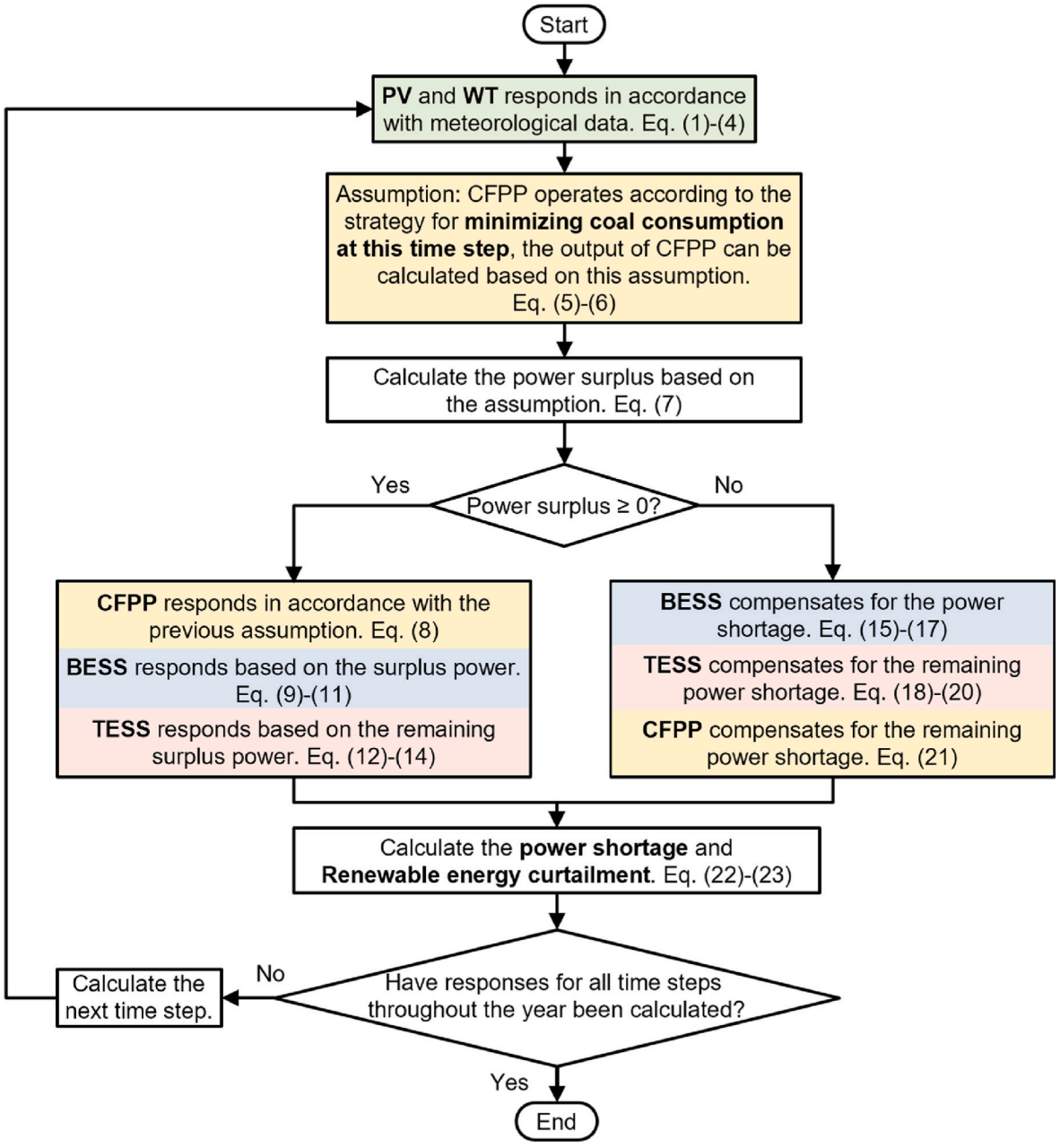


**Fig. 3.** Operation strategy of the integrated system.

$$P_{PV}(t) = Cap_{PV} \cdot \frac{GHI(t)}{GHI_{STC}} \cdot \left[1 + \sigma_{cof}(T_{cell}(t) - T_{STC})\right] \cdot \eta_{PV} \tag{1}$$

where t represents the time step, GHI is the global horizontal irradiance, $Cap_{PV}$ is the installed capacity of PV, $GHI_{STC}$ represents the GHI under standard test condition, $\sigma_{cof}$ represents temperature coefficient of PV cell, $\eta_{PV}$ represents the power supply efficiency of PV plant, $T_{STC}$ is PV cell temperature under standard test condition, and $T_{cell}$ is PV cell temperature under current condition, which can be calculated via Eq. (2).

$$T_{cell}(t) = T_{env}(t) + \frac{T_{NOCT} - 20}{800} \cdot GHI(t) \tag{2}$$

where $T_{env}$ is the environmental temperature, and $T_{NOCT}$ is the normal operation cell temperature.

The WT power output $P_{WT}$ is calculated by Eq. (3) [32–34].

$$P_{WT}(t) = \begin{cases} 0, v(t) \le v_{cut,in} \text{ or } v(t) \ge v_{cut,out} \\ Cap_{WT} \cdot \eta_{WT} \cdot \dfrac{v(t)^3 - v_{cut,in}^3}{v_{rated}^3 - v_{cut,in}^3}, v_{cut,in} < v(t) \le v_{rated} \\ Cap_{WT} \cdot \eta_{WT} \cdot v_{rated} < v(t) < v_{cut,out} \end{cases} \tag{3}$$

where $Cap_{WT}$ is the installed capacity of WT, $\eta_{WT}$ is the power supply efficiency of WT plant, $v_{cut,in}$ is the cut-in wind speed, $v_{cut,out}$ is the cut-out wind speed, $v_{rated}$ is the rated wind speed, $v(t)$ is the actual wind speed at hub height, which can be calculated via Eq. (4):

$$v(t) = v_{raw}(t) \cdot \left(\frac{h}{h_{raw}}\right)^e \tag{4}$$

where $v_{raw}(t)$ represents the wind speed at $h_{raw}$ (2m [35]), h is hub height, and e represents the wind shear exponent, which is set at 1/7

[36–38].

*3.2.2. Calculate the response of CFPP based on the assumption*

To achieve the lowest $CO_2$ emission for this time step, assume that CFPP operates based on the strategy for minimizing coal consumption. This strategy is working as Eq. (5).

Assume that CFPP operates at its minimum load:

$$P_{CFPP,min}(t) = \max\begin{cases} Cap_{CFPP}\cdot\gamma_{minimum}\cdot\eta_{CFPP,supply} \\ P_{CFPP}(t-1) - Cap_{CFPP}\cdot\eta_{CFPP,supply}\cdot\gamma_{ramp} \end{cases} \quad (5)$$

where $P_{CFPP,min}$ is the power output of CFPP when operating at its minimum load, $Cap_{CFPP}$ is the installed capacity of CFPP, $\gamma_{minimum}$ is minimum load rate of CFPP, $r_{ramp\ rate}$ represents the ramp rate of CFPP, $\eta_{CFPP,supply}$ is the power supply efficiency of CFPP and can be calculated using Eq. (6).

$$\eta_{CFPP,supply} = 1 - \xi_{self} \quad (6)$$

where $\xi_{self}$ is the comprehensive-electricity self-consumption rate of CFPP.

The above calculations are based on the assumption of "minimizing coal consumption at this time step". Subsequently, it is crucial to verify whether the assumption can meet the power demand.

*3.2.3. Verify the assumption and calculate the response of other devices*

After operating according to the above assumption, the power surplus that exceeds the power demand at this time step can be calculated using Eq. (7).

$$P_{surplus}(t) = P_{PV}(t) + P_{WT}(t) + P_{CFPP,min}(t) - P_{demand}(t) \quad (7)$$

where $P_{surplus}$ is the power surplus, $P_{demand}$ is the power demand.

Next, it is necessary to categorically discuss based on the value of power surplus.

*3.2.3.1. 1)* $\mathbf{P_{surplus}(t) \geq 0}$.

(1) CFPP responds in accordance with the previous assumption.

The output of CFPP can be calculated using Eq. (8).

$$P_{CFPP}(t) = P_{CFPP,min}(t) \quad (8)$$

(2) BESS responds based on the surplus power.

Since there is a power surplus at this time step, it is unnecessary for BESS to discharge, the discharge power of BESS is zero.

$$P_{BESS,dch}(t) = 0 \quad (9)$$

The charge power of BESS can be calculated using Eq. (10).

$$P_{BESS,ch}(t) = \min\begin{cases} P_{surplus}(t) \\ Cap_{BESS,PCS} \\ \dfrac{Cap_{BESS,storage} - E_{BESS}(t-1)}{\eta_{BESS,ch}} \end{cases} \quad (10)$$

where $Cap_{BESS,PCS}$ represents PCS capacity of BESS, $Cap_{BESS,storage}$ represents storage capacity of BESS, $E_{BESS}$ is the remaining energy stored in BESS, $\eta_{BESS,ch}$ is the charge efficiency of BESS.

The remaining energy stored in BESS is updated by using Eq. (11), based on its charge and discharge power.

$$E_{BESS}(t) = E_{BESS}(t-1) + P_{BESS,ch}(t)\cdot\eta_{BESS,ch} \quad (11)$$

where $\eta_{BESS,dch}$ is the discharge efficiency of BESS.

(3) TESS responds based on the remaining surplus power.

Since there is a power surplus at this time step, it is unnecessary for TESS to discharge, the discharge power of TESS is zero.

$$P_{TESS,dch}(t) = 0 \quad (12)$$

If there is still surplus renewable power from RE system, the TESS will be the next to respond, transforming the surplus power into thermal energy. The charge power of TESS can be calculated using Eq. (13).

$$P_{TESS,ch}(t) = \min\begin{cases} P_{surplus}(t) + P_{BESS,ch}(t) \\ Cap_{TESS,ch} \\ \dfrac{Cap_{TESS,storage} - E_{TESS}(t-1)}{\eta_{TESS,ch}} \end{cases} \quad (13)$$

where $Cap_{TESS,ch}$ is the charge capacity of TESS, $Cap_{TESS,storage}$ is storage capacity of TESS, $E_{TESS}$ is the remaining energy stored in TESS, $\eta_{TESS,ch}$ is the charge efficiency of TESS.

The remaining energy stored in TESS is updated by using Eq. (14), based on its charge and discharge power.

$$E_{TESS}(t) = E_{TESS}(t-1) + P_{TESS,ch}(t)\cdot\eta_{TESS,ch} \quad (14)$$

where $\eta_{TESS,dch}$ is the discharge efficiency of TESS.

*3.2.3.2. 2)* $\mathbf{P_{surplus}(t) < 0}$.

(1) BESS compensates for the power shortage.

Since the power output of BESS is zero-carbon, BESS takes priority in compensating for power shortage. The discharge power of BESS can be calculated using Eq. (15).

$$P_{BESS,dch}(t) = \min\begin{cases} -P_{surplus}(t) \\ Cap_{BESS,PCS} \\ E_{BESS}(t-1)\cdot\eta_{BESS,dch} \end{cases} \quad (15)$$

Since there is a power shortage at this time step, the charge power of BESS is zero.

$$P_{BESS,ch}(t) = 0 \quad (16)$$

The remaining energy stored in BESS is updated by using Eq. (17), based on its charge and discharge power.

$$E_{BESS}(t) = E_{BESS}(t-1) - \frac{P_{BESS,dch}(t)}{\eta_{BESS,dch}} \quad (17)$$

(2) TESS compensates for the remaining power shortage.

Similarly, the discharge power of TESS can be calculated using Eq. (18).

$$P_{TESS,dch}(t) = \min\begin{cases} -P_{surplus}(t) - P_{BESS,dch}(t) \\ Cap_{TESS,dch} \\ E_{TESS}(t-1)\cdot\eta_{TESS,dch} \end{cases} \quad (18)$$

Since there is a remaining power shortage at this time step, the charge power of TESS is zero.

$$P_{TESS,ch}(t) = 0 \quad (19)$$

The remaining energy stored in TESS is updated by using Eq. (20), based on its charge and discharge power.

$$E_{TESS}(t) = E_{TESS}(t-1) - \frac{P_{TESS,dch}(t)}{\eta_{TESS,dch}} \quad (20)$$

(3) CFPP compensates for the remaining power shortage.

If the discharge of the TESS is insufficient to cover the remaining power shortage, the CFPP will continue to fill the remaining shortage. The power of CFPP can be calculated using Eq. (21).

$$P_{CFPP}(t) = \min\begin{cases} -P_{surplus}(t) - P_{BESS,dch}(t) - P_{TESS,dch}(t) + P_{CFPP,min}(t) \\ Cap_{CFPP}\cdot\eta_{CFPP,supply} \\ P_{CFPP}(t-1) + Cap_{CFPP}\cdot\eta_{CFPP,supply}\cdot\gamma_{ramp} \end{cases} \tag{21}$$

### 3.2.4. Calculate the power shortage and RE curtailment

The power shortage at this time step can be calculated using Eq. (22).

$$P_{shortage}(t) = \max\begin{cases} 0 \\ P_{demand}(t) - P_{PV}(t) - P_{WT}(t) - P_{BESS,dch}(t) - P_{TESS,dch}(t) - P_{CFPP}(t) \end{cases} \tag{22}$$

If all energy storage systems (BESS and TESS) are fully charged and cannot accept more power, any additional surplus energy will be curtailed. The RE curtailment at this time step can be calculated using Eq. (23).

$$P_{curtailment}(t) = P_{surplus}(t) - P_{BESS,ch}(t) - P_{TESS,ch}(t) \tag{23}$$

### 3.2.5. Complete calculations for all time steps throughout the year

After completing calculations from 3.2.1 to 3.2.4, the operational status of all devices for this time step has been determined. If calculations have been completed for all time steps throughout the year, the calculation process ends. Otherwise, calculations for the next time step will be initiated.

## 3.3. Evaluation metrics

### 3.3.1. LCOE

The LCOE serves as a prevalent metric for assessing policy choices related to distinct support measures for fossil energy and renewable energy power production [17,39]. The methodology employed in this research to calculate LCOE is expressed through Eq. (24):

$$LCOE = \frac{\sum_i \left[ I_i \times \frac{r_i(1+r_i)^{N_i}}{(1+r_i)^{N_i}-1} + (OM_i + V_i) \right]}{\sum_t \left[ P_{demand}(t) - P_{shortage}(t) \right]} \tag{24}$$

where the subscript i represents different sub-system of the integrated system, I is the initial investment cost, OM is the annual fixed operation and maintenance cost, V is the annual variable operation cost (coal cost), N is the lifetime, and r is the discount rate, which is set to 8 % [40–42] in this study.

The initial investment cost I and annual fixed operation and maintenance cost OM can be calculated using Eqs. (25) and (26).

$$I = Cap \times UI \tag{25}$$

$$OM = I \times k \tag{26}$$

where Cap is the installed capacity of sub-system, UI is the unit investment cost of sub-system, k is the annual fixed O&M cost ratio of sub-system.

The annual variable operation cost V can be calculated using Eq. (27).

$$V = p_{coal} \times m_{coal} \tag{27}$$

where $p_{coal}$ represents the price of coal, t is the hour time, $m_{coal}$ represents mass consumption of coal, $m_{coal}$ can be calculated through Eq. (28):

$$m_{coal} = \sum\nolimits_t P_{CFPP}(t) \times \beta_{CFPP}\left(\frac{P_{CFPP}(t)}{Cap_{CFPP}\cdot\eta_{CFPP,supply}}\right) \tag{28}$$

where $\beta_{CFPP}$ is the standard coal consumption for power supply of CFPP. The value of $\beta_{CFPP}$ typically vary with the load rate of CFPP, as illustrated in Fig. 4. At optimal operating condition, $\beta_{CFPP}$ reaches its minimum value of 280.5 g/kWh [43]. The functional relationship between standard coal consumption and CFPP load rate has been established through the correlation developed by Dong et al. [44], which accurately reflected the variation of $\beta_{CFPP}$ across different operating conditions.

### 3.3.2. Power supply reliability

The power supply reliability is introduced to assess the safety capabilities of the integrated power system, which can be calculated through Eq. (29):

$$reliability = 1 - \frac{\sum_t P_{shortage}(t)}{\sum_t P_{demand}(t)} \tag{29}$$

### 3.3.3. Specific $CO_2$ emission

The average $CO_2$ emitted per kWh of electricity produced is defined as specific $CO_2$ emission, which can be calculated through Eq. (30):

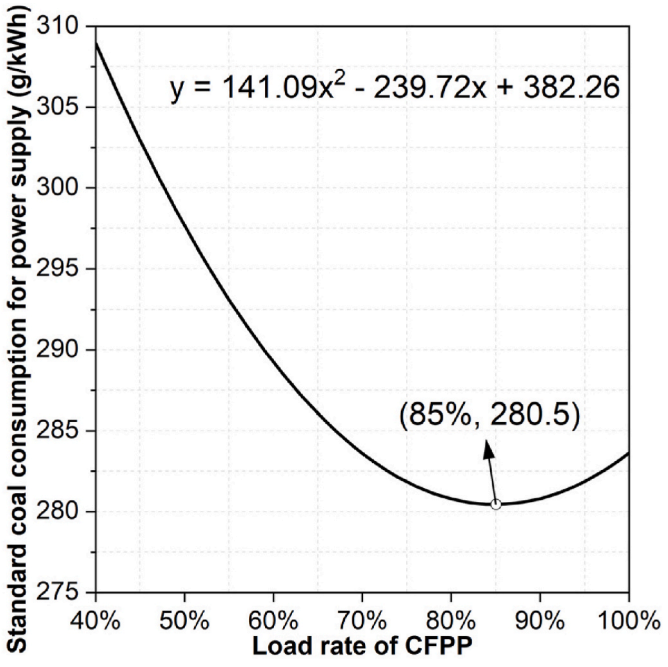


**Fig. 4.** Functional relationship between standard coal consumption and CFPP load rate.

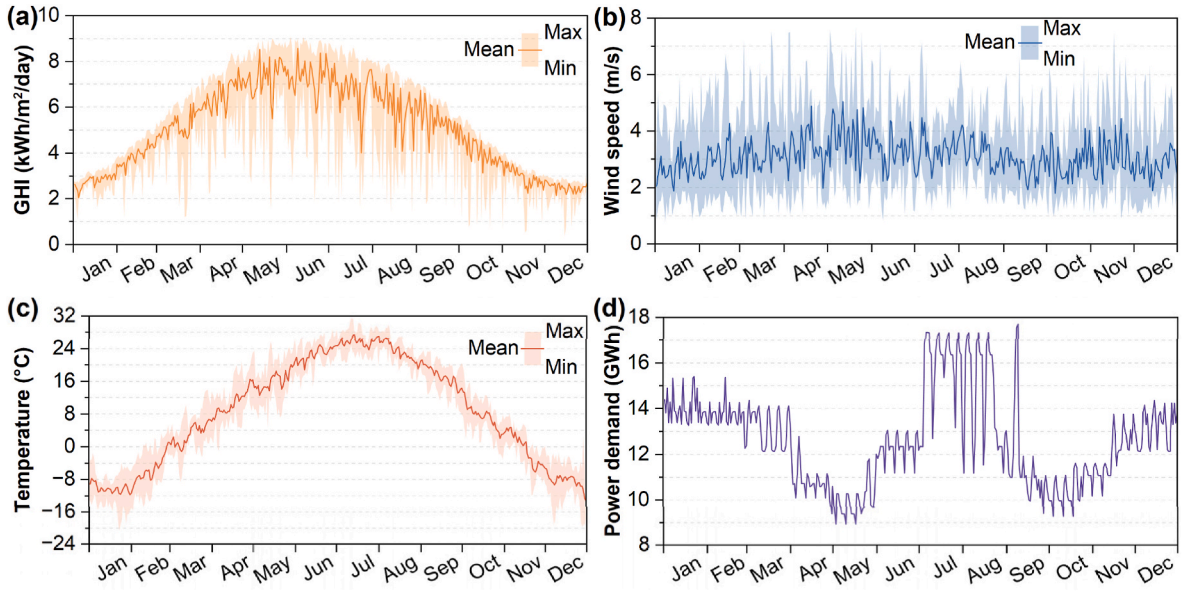


**Fig. 5.** Daily values of meteorological data and power demand.

$$\alpha = \frac{m_{coal} \times \theta_{coal}}{\sum_{t=1}^{8760}\left(P_{demand}(t) - P_{shortage}(t)\right)} \quad (30)$$

where $\theta_{coal}$ represents $CO_2$ emission factor of coal.

### 3.4. Input data and assumptions

This study selected Alxa Left Banner (40.16°N, 104.81°E), Inner Mongolia, abundant in solar and wind energy resources, as the study location. The meteorological data (GHI, wind speed and temperature) was obtained from NSRDB [35], with a time resolution of 10 min.

Fig. 5 (a) shows the daily cumulative of GHI over the past five years. The bands in the figure represent the maximum and minimum daily total GHI over the past five years. As can be observed, the local GHI tends to be higher during the summer (June to August) and lower in winter (December to February). Similarly, Fig. 5 (b) and (c) display the daily average wind speed and environmental temperature, respectively, over the past five years. The wind speed fluctuates around 3 m/s throughout the year, while the environmental temperature exhibits a pattern similar to that of GHI, with higher values in summer and lower values in winter. The five-year averaged meteorological data for these variables will be utilized when conducting subsequent system operation simulations, to mitigate the impact of seasonal variations.

The power demand shown in Fig. 5 (d) is obtained by scaling a typical normalized power demand to 1000 MW, which is sourced from the National Grid [45]. The average power demand during the summer is the highest, while the spring (February to May) and autumn (September to November) seasons exhibit the lowest average power demand.

To ensure the techno-economic parameters accurately reflect actual conditions, comprehensive data gathering was undertaken. By reviewing relevant literature and analyzing actual projects, the baseline values utilized in this study were determined. Tables 2 and 3 present the reference values and baseline values for different sub-systems. Notably, values lacking cited sources were derived from investigations of actual projects. Exchange rate conversions for currencies are calculated using average international exchange rate over the period from January to December 2023, where 1 Chinese Yuan (CNY) is equivalent to approximately 0.1407 United States Dollars (USD).

**Table 2**
Values for the photovoltaic system, wind turbine, and coal-fired power plant.

| Parameters | Unit | Reference value | Baseline value |
|---|---|---|---|
| *Photovoltaic system* | | | |
| Unit investment cost | CNY/kW | 4239 [43] | 4239 |
| Annual fixed O&M cost ratio | % | 2 [36], 3 [46] | 2.5 |
| Power supply efficiency | % | 80 [18,47] | 80 |
| Temperature coefficient | %/°C | −0.34 [48] | −0.34 |
| Normal operation cell temperature | °C | 20 [48] | 20 |
| GHI under standard test condition | W/m$^2$ | 1000 [48] | 1000 |
| PV cell temperature under standard test condition | °C | 25 [48] | 25 |
| Lifetime | year | 25 [48] | 25 |
| *Wind Turbine* | | | |
| Unit investment cost | CNY/kW | 5217 [43] | 5217 |
| Annual fixed O&M cost ratio | % | 3.1 [36], 2.4 [34] | 3 |
| Power supply efficiency | % | – | 80 |
| Cut-in speed | m/s | 2 [49] | 2 |
| Cut-out speed | m/s | 9 [49] | 9 |
| Rated speed | m/s | 18 [49] | 18 |
| Hub height | m | 100 [49] | 100 |
| Lifetime | year | ≥20 [49] | 25 |
| *Coal-fired power plant* | | | |
| Unit investment cost | CNY/kW | 3309 [50], 3317 [51], 3590 [52], 3536–4542 [43] | 3536 |
| Annual fixed O&M cost ratio | % | 4.5 [53] | 4.5 |
| Comprehensive-electricity self-consumption rate | % | 4.1 % [50], 4.65 % [51], 3.97 %–6.44 % [43] | 3.97 % |
| Minimum load rate | % | 30 [54,55], 40 [54], 40–50 [56] | 40 |
| Ramp rate | %/min | 1-2 [54] | 1 |
| Lifetime | year | 40 [57,58] | 40 |
| Coal heat value | kJ/kg | 29307 (standard coal) | 29307 |
| Coal price | CNY/t | 1000 [59] | 1000 |
| $CO_2$ emission factor of standard coal | kg $CO_2$/kg | 2.72 [51,60], 2.61–2.74 [61][a] | 2.7 |

[a] The $CO_2$ emission factor is converted based on heat value.

**Table 3**
Values for different energy storage technologies.

| Parameters | Unit | Reference data | Baseline value |
|---|---|---|---|
| *Battery energy storage* | | | |
| Unit investment cost of PCS part | CNY/kW | 300 [62] | 300 |
| Unit investment cost of storage part | CNY/kWh | 1600[a] [63] | 1500 |
| Annual fixed O&M cost ratio | % | 2 [18], 0.43 [64] | 1 |
| Charge efficiency | % | 95 [46,64] | 95 |
| Discharge efficiency | % | 95 [17,46,64] | 95 |
| Lifetime of PCS part | year | 10 [44,62] | 10 |
| Lifetime of storage part | year | 16 [64] | 10 |
| *Thermal energy storage* | | | |
| Unit investment cost of charge part | CNY/kW | 1000 [19], 700 [65], 759 | 800 |
| Unit investment cost of discharge part | CNY/kW | 1750 (estimated by Ref. [50]) | 1750 |
| Unit investment cost of storage part | CNY/kWh | 600 [64], 210 [65], 338–504 | 400 |
| Annual fixed O&M cost ratio | % | 2 [64] | 2 |
| Charge efficiency (power to heat efficiency) | % | 100 [65] | 95 (considering heat dissipation) |
| Discharge efficiency (heat to power efficiency) | % | 47.28 [53] | 47.28 |
| Lifetime of PCS part | year | 30 [65], 15 [19,36], 20 | 30 |
| Lifetime of storage part | year | 30 [36,64], 25 [19,36], 20 | 30 |

[a] Including PCS part.

## 4. Results and discussion

### 4.1. Comparative techno-economic analysis of various cases

In this section, the optimal configuration (Case 6), obtained through the aforementioned steps, was compared with five other cases to highlight the advantages of the optimal configuration and to explore the specific reasons for these advantages. The capacity configurations of each system were adjusted progressively across the cases to investigate the influence of different power generation mixes. The main characteristics of each case are outlined below.

**Case 1.** Only coal-fired power plant.

**Table 4**
Configurations of various cases.

| Sub-system | Case 1 | Case 2 | Case 3 | Case 4 | Case 5 | Case 6 (Optimal) |
|---|---|---|---|---|---|---|
| **CFPP** | 1000 MW | 800 MW | 800 MW | 600 MW | 600 MW | 442 MW |
| **PV** | / | 400 MW | 800 MW | 800 MW | 1200 MW | 1167 MW |
| **WT** | / | 400 MW | 800 MW | 800 MW | 1200 MW | 1186 MW |
| **BESS** | | | | | | |
| PCS | / | / | / | 100 MW | 200 MW | 165 MW |
| Storage | / | / | / | 200 MWh | 400 MWh | 1083 MWh |
| **TESS** | | | | | | |
| Charge | / | / | / | 200 MW | 400 MW | 643 MW |
| Discharge | / | / | / | 200 MW | 400 MW | 194 MW |
| Storage | / | / | / | 800 MWh | 1600 MWh | 4261 MWh |

**Case 2.** On the basis of Case 1, reduce CFPP and incorporate RE systems.

**Case 3.** On the basis of Case 2, further expand installed capacity of RE systems.

**Case 4.** On the basis of Case 3, reduce CFPP while incorporating energy storage systems.

**Case 5.** On the basis of Case 4, increase both RE and energy storage capacities.

**Case 6.** The optimal configuration.

The detailed configurations of the six cases are listed in Table 4.

The specific $CO_2$ emission and LCOE for each configuration are compared in Fig. 6(a) and (b), respectively.

Compared to Case 1, Case 2 replaces a portion of CFPP with RE, effectively reducing the specific $CO_2$ emission, though this comes with a slight increase in LCOE. In contrast, comparing Case 3 with Case 2 reveals that an inappropriate increase in RE results in a significant increase in LCOE, while only marginally reducing specific $CO_2$ emission. The capacities of each sub-system need to be appropriately configured to achieve a suitable cost in carbon emissions reduction.

The comparison of Case 4 and Case 3 reveals that partially replacing CFPP with energy storage system (ESS) can lead to reductions in both specific $CO_2$ emissions and LCOE. This is because increasing the ESS capacity allows RE curtailment to be utilized to meet power demand, which in turn enables a reduction in CFPP capacity, thereby lowering both LCOE and specific $CO_2$ emission.

Compared to Case 4, the expansion of RE and ESS in Case 5 lowers specific $CO_2$ emission, but significantly increases LCOE. This further demonstrates that the capacities of each sub-system must be properly configured to achieve a balanced and cost-effective reduction in carbon emissions.

Compared to Case 5, the RE capacities in Case 6 remain nearly unchanged. However, by optimizing the configuration of ESS—adjusting both charging/discharging power and storage duration—the CFPP capacity is reduced while ensuring power supply reliability. This not only lowers LCOE but also further reduces carbon emissions.

The dashed lines in Fig. 6 represent the corresponding metrics for natural gas combined cycle power plant (NGCC). These values were obtained based on reference [53], with further consideration of the variation in natural gas consumption with load rate. The method used in Section 3.3.1 to determine the standard coal consumption of CFPP at different load rate was employed to calculate the natural gas consumption of NGCC under different load rate. The specific $CO_2$ emission of Case 6 is equivalent to that of the NGCC, demonstrating a significant 56.4 % reduction compared to Case 1, which represents a conventional CFPP scenario. Furthermore, the LCOE of Case 6 is 0.563 CNY/kWh, representing a 12.4 % reduction compared to the NGCC. These findings underscore that Case 6, as the optimal configuration, presents a cost-effective and efficient solution for carbon emission mitigation.

### 4.2. Operational analysis of the proposed integrated power system

This section presents the analyzed operation schedules of optimal configurations during typical days, aimed at validating the rationality of the system's operation.

Fig. 7 (a) illustrates the power balance across different months. From January to March, the power demand is relatively stable, while the power output from RE gradually increases. Consequently, the output from CFPP gradually decreases, therefore, the specific $CO_2$ emission decreases month by month, as shown in Fig. 7 (b).

During April, May, and June, when power demand is relatively low, the wind and solar sources exhibit abundant availability, resulting in a notably higher power output from RE. Consequently, the power output from CFPP undergoes a substantial reduction. This low power demand

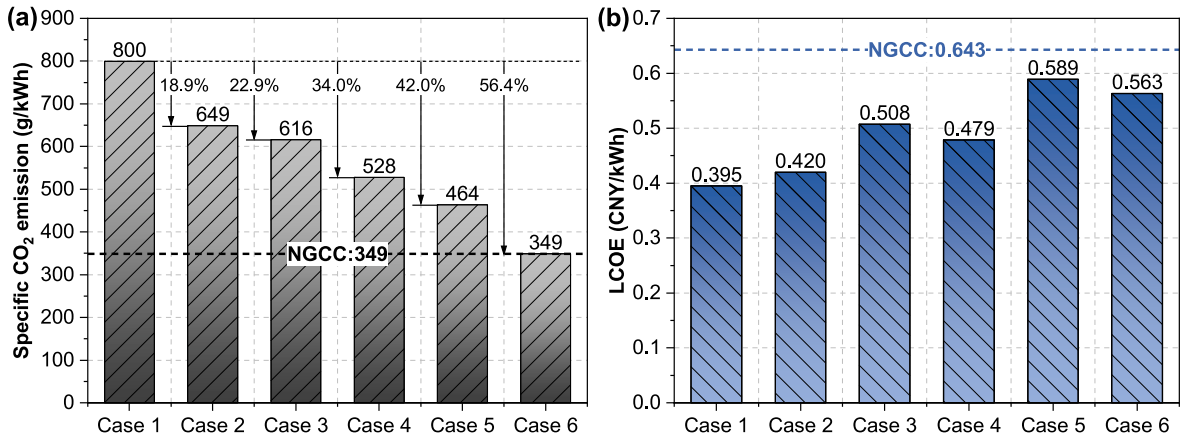


**Fig. 6.** (a) LCOE and (b) specific $CO_2$ emission comparison of different cases.

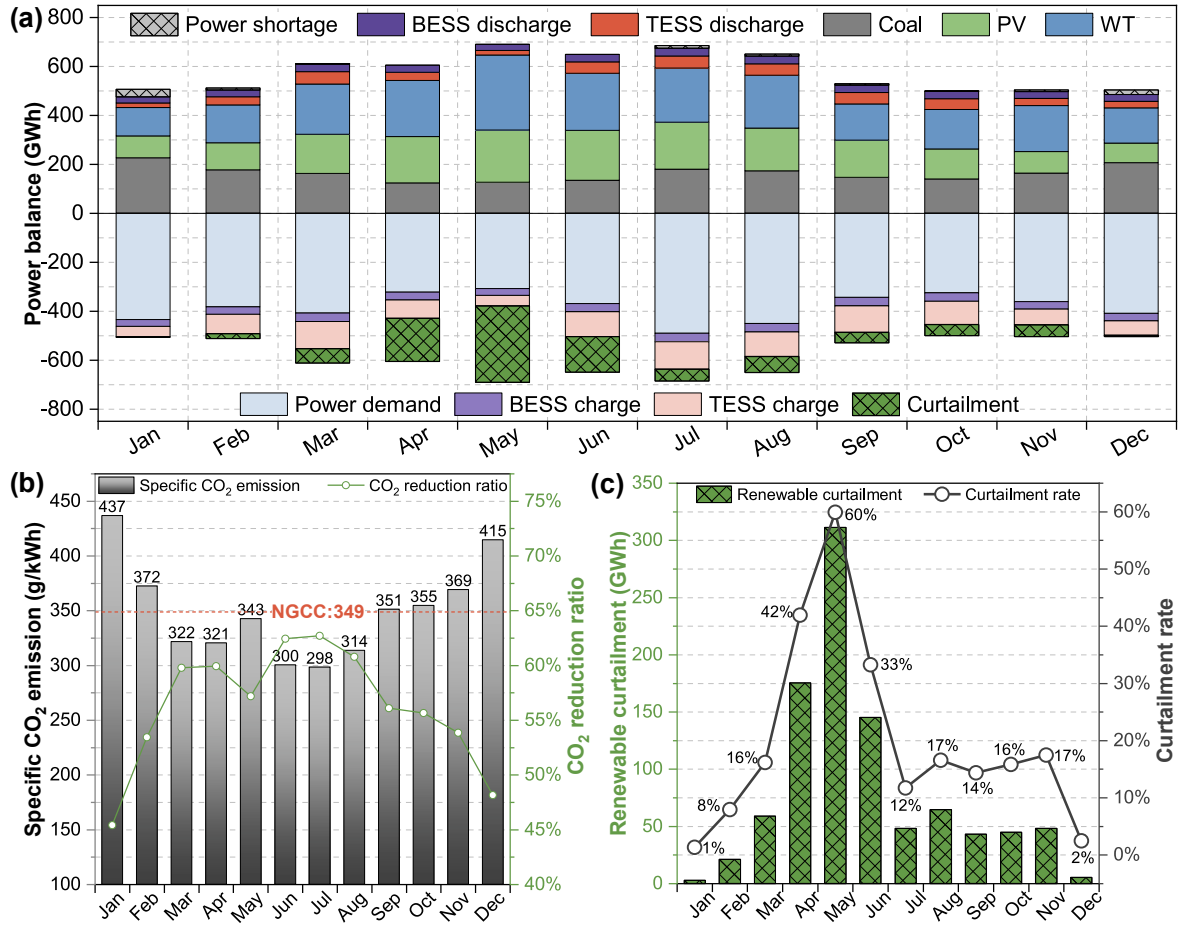


**Fig. 7.** Monthly overview: (a) power balance, (b) specific $CO_2$ emission and reduction ratio, (c) renewable curtailment and curtailment rate.

scenario also leads to a significant proportion of RE-generated power remaining unutilized, resulting in extensive renewable curtailment, as illustrated in Fig. 7 (c). Specifically, the renewable curtailment rates (the proportion of unutilized RE-generated power in the total power output from renewable energy) for April, May, and June were 42 %, 60 %, and 33 %, respectively. Although the installation of additional ESS could potentially reduce these curtailments, the current installed capacity has already been optimized. Adding more ESS, even if it leads to more effective utilization of the renewable curtailment, would significantly increase the LCOE, making it an unprofitable endeavor.

In May, a noticeable increase in specific $CO_2$ emission was observed, as depicted in Fig. 7 (b). This increase can be attributed to that while power demand reached its minimum level during this month, the minimum load rate constraints imposed by CFPP prevented a further decrease in its power output. Consequently, the relative share of CFPP within the total power output increased, thereby contributing to the increase of specific $CO_2$ emission.

During July and August, there is a notable increase in power demand, resulting in the effective utilization of RE output and a subsequent reduction in curtailment. The power shortage predominantly emerged in

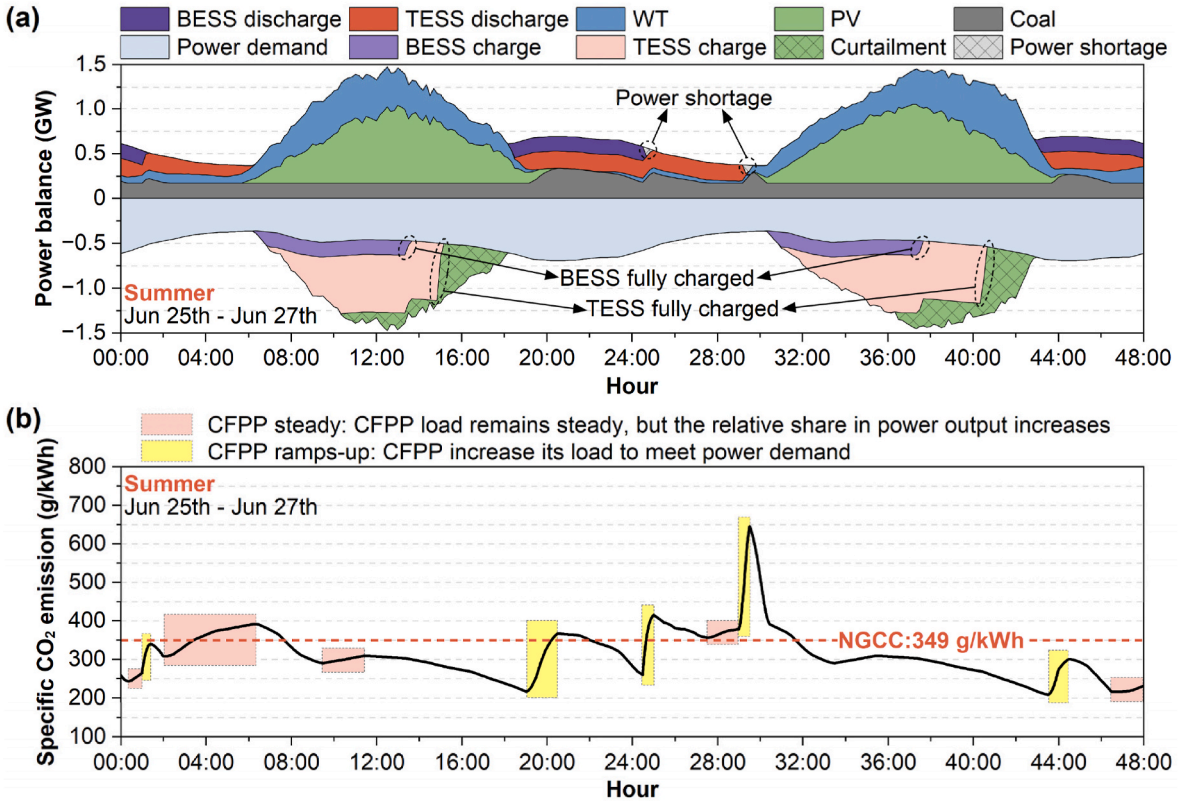


**Fig. 8.** Selected 48-h(a) operational schedules and (b) specific $CO_2$ emission profiles for summer.

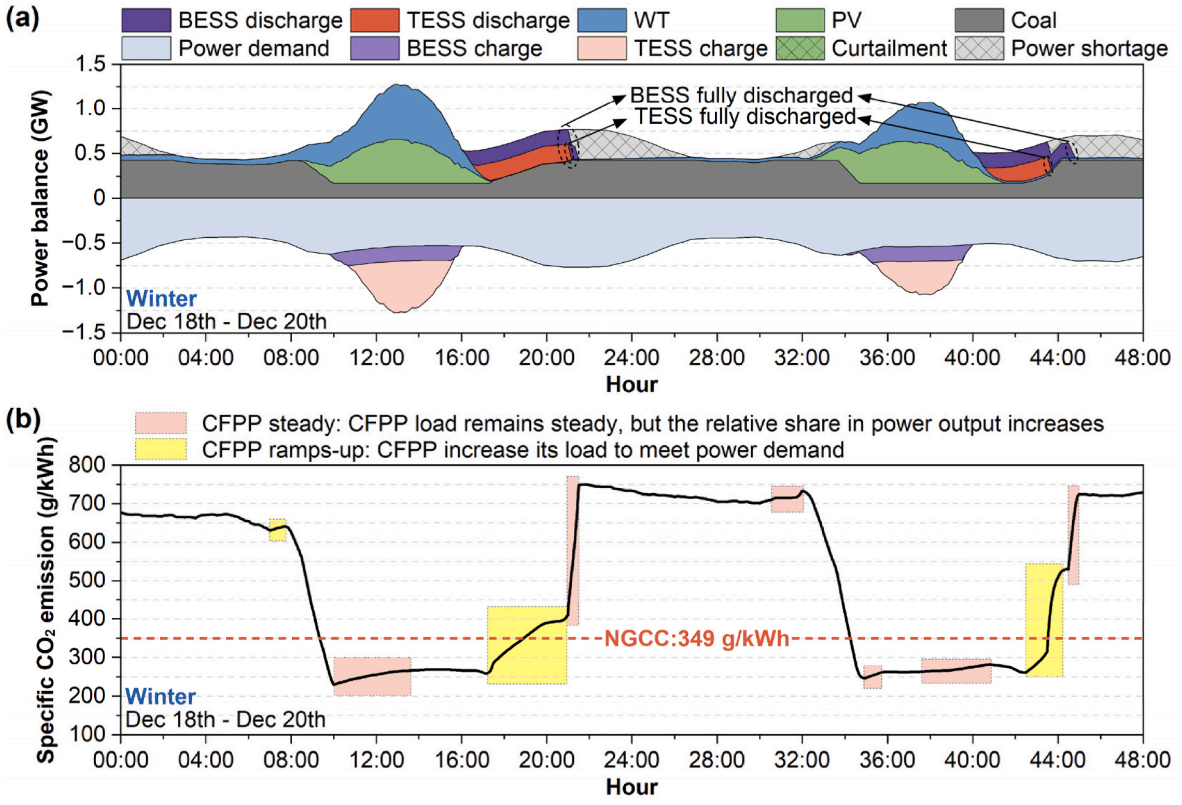


**Fig. 9.** Selected 48-h(a) operational schedules and (b) specific $CO_2$ emission profiles for winter.

December and January, attributable to the insufficiency of wind and solar resources during these periods, whereby CFPP alone was inadequate to meet the power demand.

The red dashed line in Fig. 7 (b) represents the specific $CO_2$ emission of NGCC. Notably, from March through August, the proposed integrated low-carbon power system consistently exhibited a lower specific $CO_2$ emission compared to that of the NGCC, highlighting its environmental superiority during these months.

Fig. 8 (a) depicts the operational schedules for the integrated power system from June 25th to June 27th, characterized by abundant wind and solar energy resources. During daytime, the BESS and TESS are typically fully charged, and excess power becomes curtailment. Conversely, at night, BESS and TESS discharge to meet the power demand, but there are occasional minor instances of power shortage. The main reasons contributing to these power shortages can be attributed to the following:

First, the power shortage occurs when BESS and TESS are fully discharged, indicating that the ESS capacity is a significant reason for the power shortage. However, it should be noted that the ESS capacity is already sufficient to meet the reliability constraint ($\geq$98 %). Further increasing the ESS capacity would result in an unnecessary increase in LCOE.

Secondly, constrained by the ramp rate, CFPP always requires a temporal window to raise its load to compensate for the power shortage. Consequently, during this transitional period of load ramp-up, a temporary power shortage inevitably arises.

Fig. 8 (b) presents a comprehensive analysis of the system's specific $CO_2$ emission variations over the two days. The increase in specific $CO_2$ emission can be attributed to two distinct load states of CFPP: steady (as indicated by the red area) and ramp-up (as indicated by the yellow area).

During periods of steady CFPP load, the observed rise in specific $CO_2$ emission occurs when the power demand gradually decreases, yet the CFPP maintains its minimum operation load. This scenario leads to an increased relative share of CFPP output within the total power output, ultimately contributing to the elevation of specific $CO_2$ emission.

Conversely, the CFPP ramp-up scenario typically arises due to the insufficiency of zero-carbon power from RE and ESS. The CFPP must ramp up to meet the power demand, increasing both its absolute and relative share of the total power output, which further elevates $CO_2$ emissions.

Overall, the specific $CO_2$ emission of the system fluctuates slightly around the reference value of NGCC, as depicted by red dashed line in Fig. 8 (b).

Fig. 9 (a) illustrates the operational schedules for December 18th to December 20th, highlighting the challenges encountered during the winter season when RE resources are insufficient. In this situation, the energy stored in ESS during the daytime is inadequate. Consequently, the BESS and TESS are typically fully discharged by approximately 22:00. Even if CFPP operates at its maximum load, it is still unable to fully meet the power demand, resulting in a significant amount of power shortage.

Fig. 9 (b) illustrates the significant fluctuations in specific $CO_2$ emissions during the winter, with daytime bellowing 300g/kWh while nighttime approaching 800g/kWh. Compared to summer, the fluctuations in specific $CO_2$ emissions are more noticeable in winter due to greater power shortages at night. A substantial portion of power output is supplied by CFPP at night, ultimately, the specific $CO_2$ emission increased significantly.

### 4.3. System performance across time via probabilistic distribution analysis

An analysis of probabilistic distribution is conducted in this section to examine the daily variations in key indicators across different seasons.

#### 4.3.1. Specific $CO_2$ emission distribution

Fig. 10 presents the seasonal variability in the frequency distribution of specific $CO_2$ emission. The hollow circles and squares in the figure indicate the mean and median values, illustrating a trend of lower emissions during summer and higher emissions during winter.

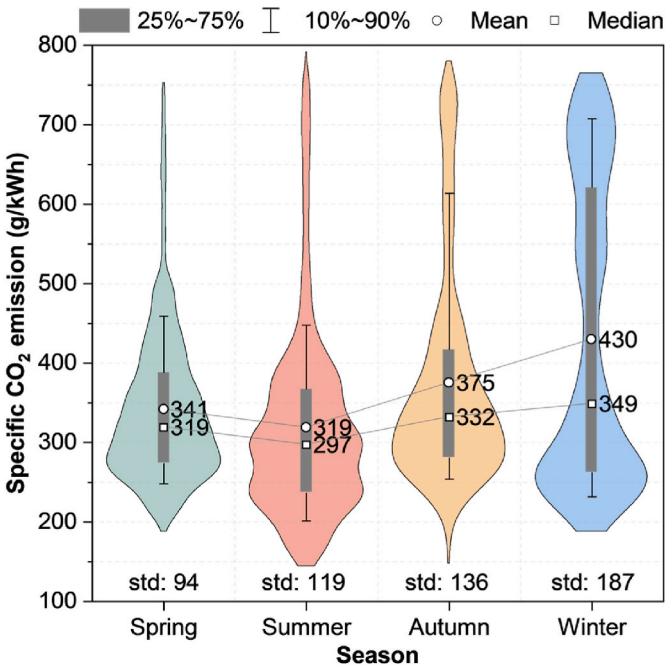


**Fig. 10.** Frequency distribution of specific $CO_2$ emission in different seasons.

The distribution curves during spring, summer, and autumn exhibit unimodal distributions, with a skew toward the range of 250–350 g/kWh, and a low proportion of values exceeding 550 g/kWh. In contrast, during winter, the distribution curve exhibits a bimodal shape, with an increased proportion of values above 550 g/kWh, and the box exhibits a broader distribution. This discrepancy is attributed to the insufficient availability of wind and solar resources, which leads to higher specific $CO_2$ emission at night. This situation also contributes to significant variations in specific $CO_2$ emission throughout the day.

Fig. 11 presents the daily variation of specific $CO_2$ emission across four seasons. From 9:00 to 18:00, a consistent trend of approximately 300 g/kWh is observed for all seasons. Notably, during spring and autumn, owing to the relatively lower power demand, as illustrated in Fig. 5 (d), a marginal elevation in specific $CO_2$ emission during this period is discernible. Conversely, during the nighttime hours from 19:00 to 8:00, the specific $CO_2$ emission increases significantly, peaking around 6:00, as the energy stored in ESS is typically fully discharged by this time, resulting in power output primarily supplied by CFPP.

In seasons with abundant wind and solar resources, namely spring, summer, and autumn, the BESS and TESS effectively compensate for the initial power shortage during the early night hours, leading to a relatively slower increase in specific $CO_2$ emission. However, during winter, the specific $CO_2$ emission rises rapidly at night, sustaining a high level with an average approximating 600 g/kWh, highlighting the heightened dependence on CFPP during this period.

These findings have significant implications for system management strategies. During spring, summer, and autumn, the integrated power system can continue to prioritize renewable energy sources to maintain low emissions. However, during winter, when renewable energy availability is reduced, more data-driven optimal power scheduling strategies need to be adopted to mitigate the carbon emissions [66]. These strategies may include combining power demand forecasting with renewable energy power output predictions to adjust the operational timeframes of CFPP, thereby minimizing emissions.

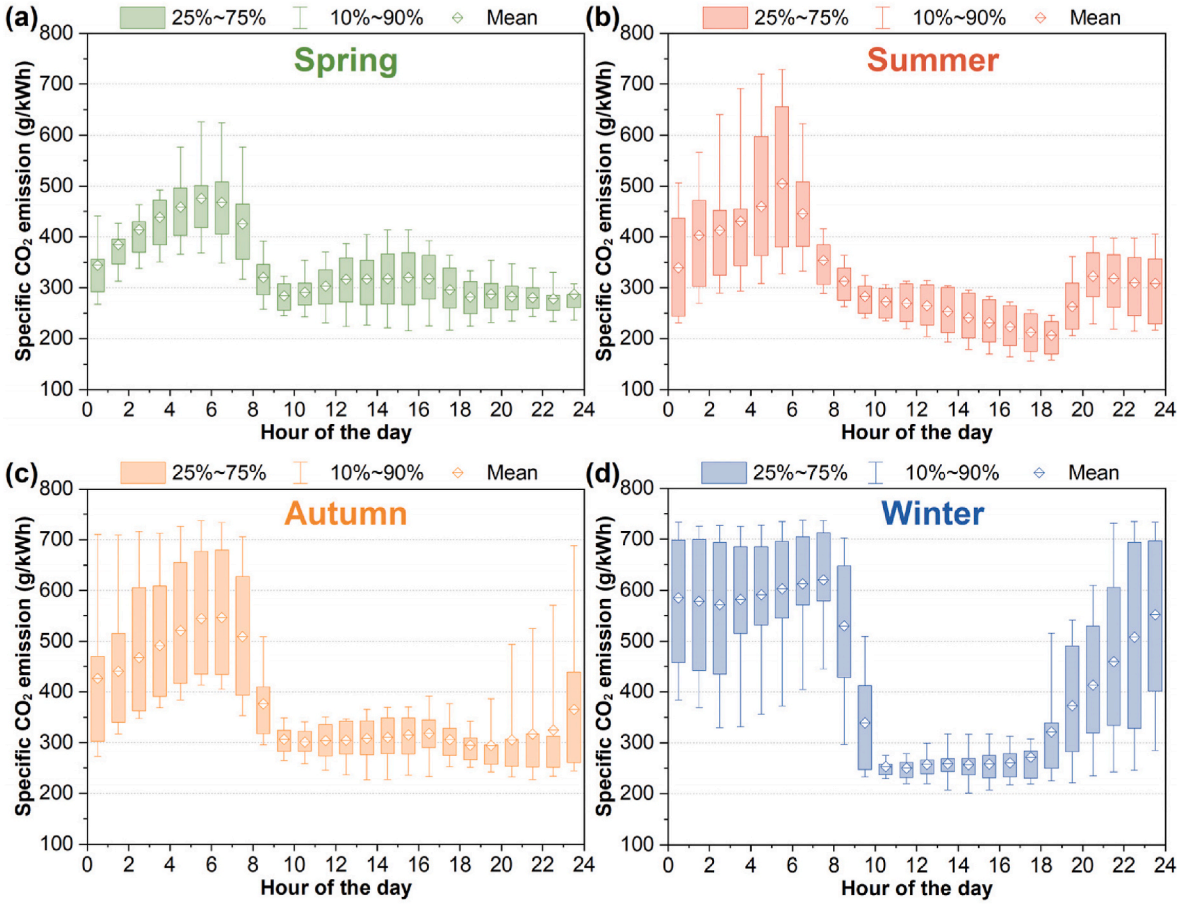


**Fig. 11.** Hourly distribution of specific $CO_2$ emission in different seasons.

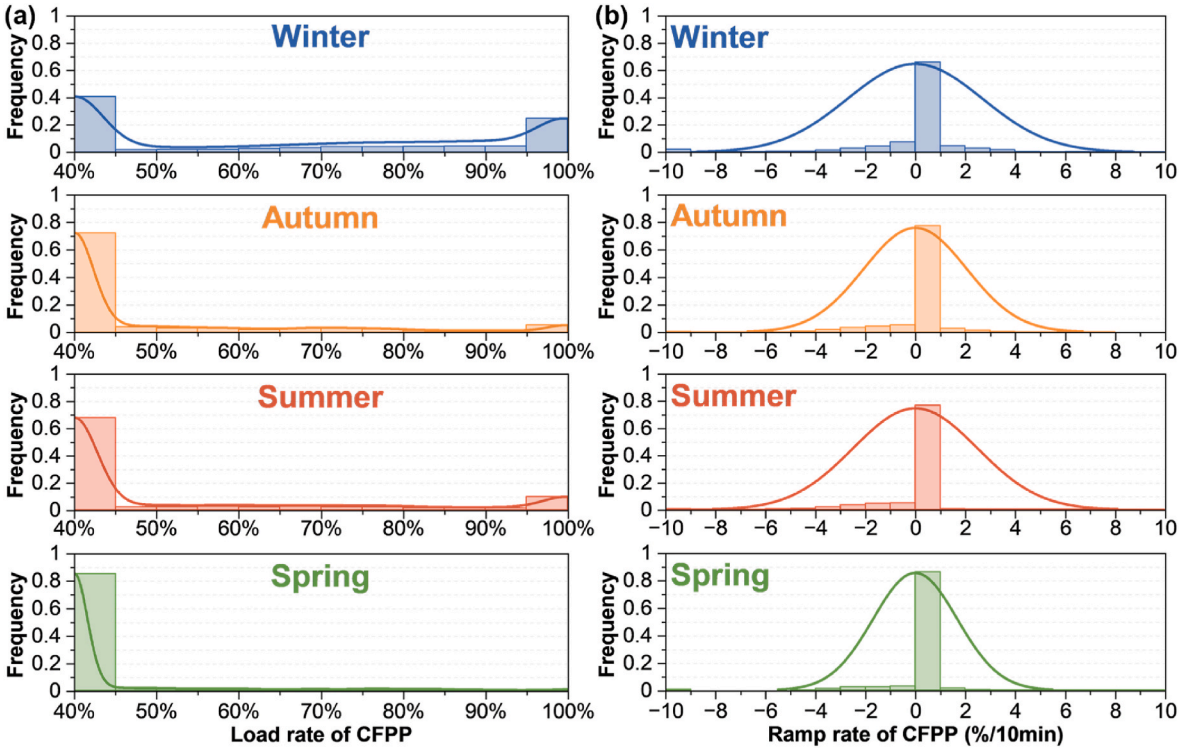


**Fig. 12.** Frequency distribution of (a) load rate and (b) ramp rate of CFPP in different seasons.

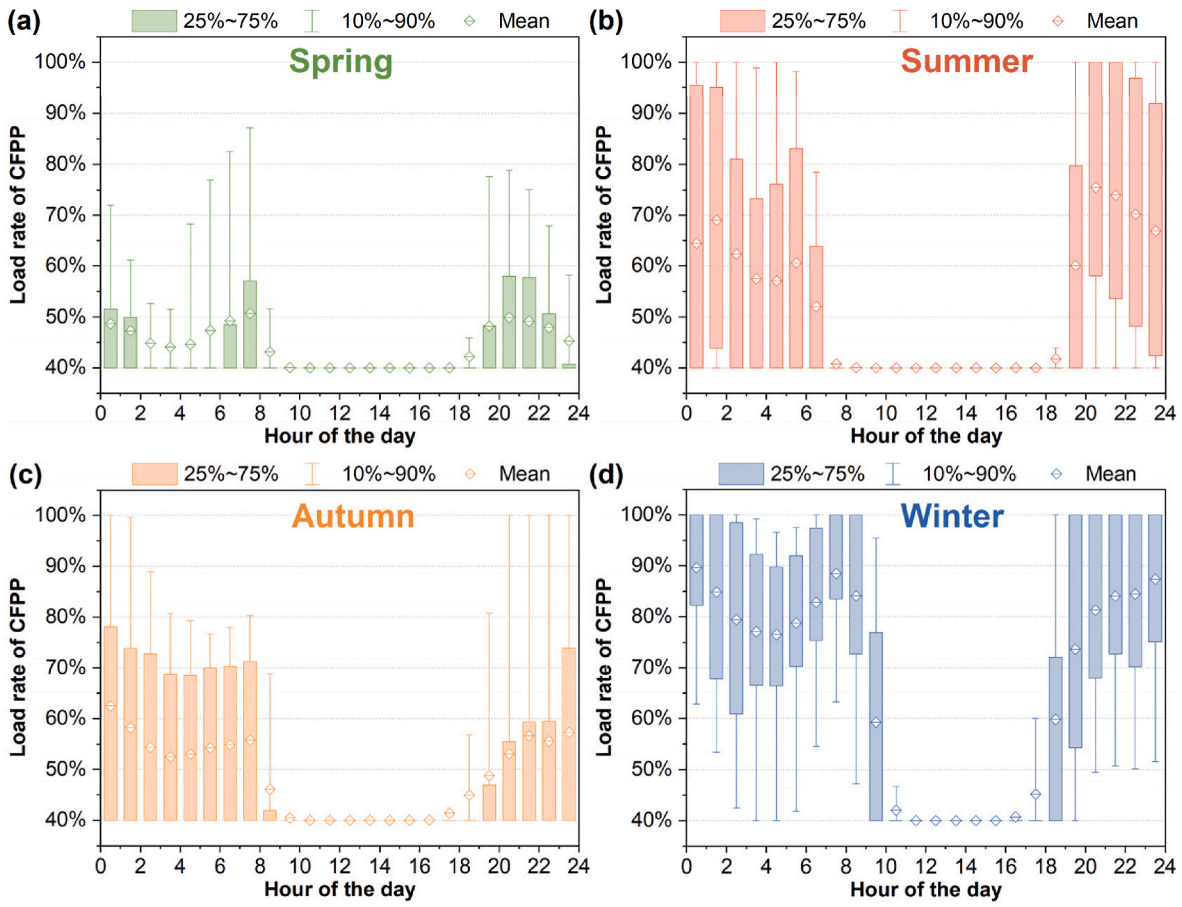


**Fig. 13.** Hourly distribution of load rate of CFPP in different seasons.

*4.3.2. Load rate distribution of coal-fired power plant*

The frequency analysis of the load rate of CFPP across the four seasons has been conducted, employing a 5 % grouping interval, as shown in Fig. 12 (a). The frequency of load rate within the 40 %–45 % range is extremely high in spring, summer, and autumn, reaching 0.85/0.68/0.72, respectively. In contrast, in winter, the frequency of load rate within this range decreases to 0.41, while the frequency of load rate between 95 % and 100 % increases to 0.25, exhibiting a "bimodal distribution". This observation underscores the different load operational scenarios for CFPP during winter, highlighting the seasonal variability in its operational characteristics.

Fig. 12 (b) illustrates that the ramp rates of CFPP are primarily concentrated around 0 %, with extreme values of −10 %/10min and 10 %/10min occurring rarely. This frequency distribution indicates that CFPP rarely participate in extensive peak shaving operations. The integrated power system demonstrates a robust capability in accommodating load variations, effectively meeting ramping requirements in most operational scenarios.

Fig. 13 presents the hourly distribution of CFPP load rate across four seasons. The average load is lowest in spring and highest in winter. The absence of visible box and whisker plots from 11:00 to 17:00 signifies an extreme concentration of sample points, revealing that CFPP consistently operates at a load rate of 40 % during this period on most days, highlighting a predictable and stable operational pattern.

During spring, summer, and autumn, CFPP maintains a minimum load of 40 % consistently from 9:00 to 18:00. However, in winter, this period of sustained minimum load undergoes a slight adjustment, shortening to encompass only the hours from 11:00 to 17:00.

During the remaining hours of the day, the broader distribution of CFPP load rate reflects the dynamic nature of its operation. This broader distribution underscores the importance of frequent peak shaving adjustments, which are necessitated by the fluctuations in renewable energy sources. CFPP must adapt its operational strategies to balance the variable output of these resources, ensuring a stable and reliable power supply.

*4.3.3. SOC distribution of energy storage systems*

Fig. 14 illustrates the seasonal variation in the hourly distribution of SOC for BESS. The SOC of BESS exhibits a predictable charging and discharging pattern, with charging predominantly occurring during daytime and discharging at night. Notably, the SOC peaks around 16:00, and the peak value in winter is significantly lower than in other seasons, reflecting the seasonal variability in renewable energy sources.

After 16:00, the power output of CFPP, PV, and WT are unable to meet power demand, therefore, the SOC gradually decreases as BESS discharges to compensate for power shortage. As the BESS discharges, the SOC gradually approaches 0 %. However, in spring, the average SOC remains above 0 % due to lower power demand and relatively abundant wind and solar resources, allowing the BESS to retain stored energy without fully discharging.

Notably, during spring, the SOC experiences a slight increase from 1:00 to 7:00, attributed to lower power demand during these hours. This leads to the power output from the WT and CFPP occasionally exceeding demand, allowing surplus power to charge the BESS and elevate its SOC.

A discharge cycle is defined as the process of SOC decreasing from 100 % to 0 %. Alternatively, if the amount of discharged energy reaches the full storage capacity, it can also be considered an equivalent discharge cycle. Therefore, the annual equivalent discharge cycles and daily average equivalent discharge cycles for each season can be calculated using Eqs. (31) and (32):

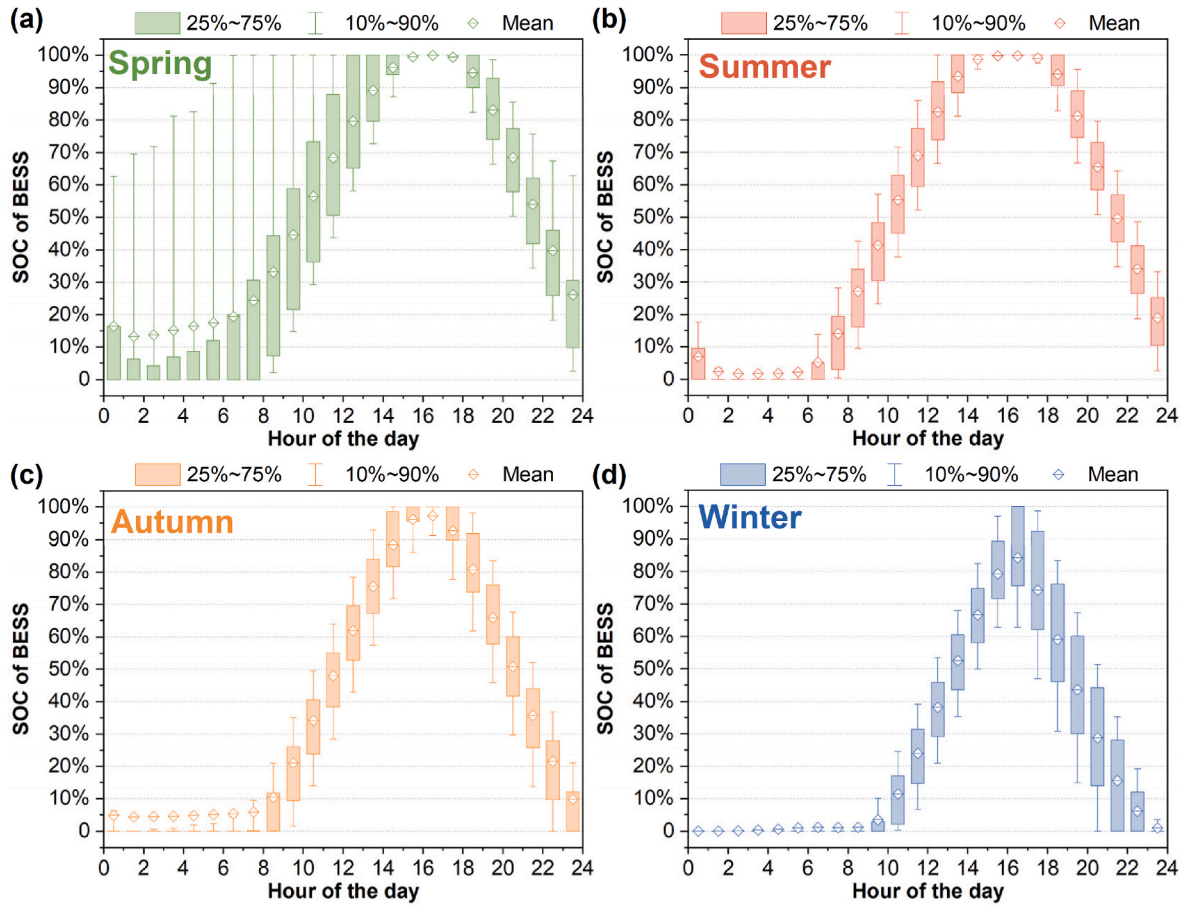


**Fig. 14.** Hourly distribution of SOC of BESS in different seasons.

$$\text{Annual equivalent discharge cycles} = \frac{\sum P_{BESS,dch}(t)}{\eta_{BESS,dch} \cdot Cap_{BESS,storage}} \quad (31)$$

$$\text{Daily average equivalent discharge cycles} = \frac{\sum P_{BESS,dch}(t)}{\eta_{BESS,dch} \cdot Cap_{BESS,storage} \cdot n_{day}} \quad (32)$$

The annual equivalent discharge cycles of the BESS reach 338, with seasonal variations in the daily average equivalent discharge cycles, specifically 0.892 in spring, 0.990 in summer, 0.952 in autumn, and 0.875 in winter. This trend indicates a more frequent charging and discharging pattern during summer, underscoring the substantial role played by the BESS in daily peak shaving operations.

The hourly distribution of SOC for TESS in different seasons are illustrated in Fig. 15. The operational pattern of TESS is similar to that of BESS, with charging occurring during the day and discharging at night, indicating its participation in daily peak shaving. However, the SOC of the TESS exhibits a broader distribution range compared to BESS, primarily due to its charging and discharging process following BESS, which makes it more affected by fluctuations in renewable resources and power demand.

The SOC of the TESS seldom reaches 0 %, which allows it to provide zero-carbon electricity during periods of power shortage. Similarly, it seldom reaches 100 %, preserving a reserve charging capacity in anticipation of abundant renewable energy availability.

The annual equivalent discharge cycles of TESS amount to 220, with seasonal variations in the daily average equivalent discharge cycles: 0.555 in spring, 0.768 in summer, 0.657 in autumn, and 0.433 in winter. These discharge cycles are significantly lower than those of the BESS, indicating a lower utilization frequency of the TESS storage part and substantial reserve capacity. Given the significantly lower investment costs for the storage part of TESS compared to the BESS, configuring a larger storage capacity for the TESS is a reasonable approach.

### 4.4. Sensitivity analysis

To identify the most critical parameters impacting the LCOE, a univariate sensitivity analysis was conducted to evaluate the proportional influence of each parameter. The sensitivity analysis employed case6, which represents the optimal configuration, as the baseline configuration. This univariate sensitivity analysis methodology involves calculating the variations in LCOE when each parameter is increased or decreased by 10 % from its baseline value. The baseline value is as specified in the last column of Tables 1–3

Fig. 16 illustrates that the unit investment cost of WT is the most influential parameter on LCOE, with coal price following closely. Although the variations caused by the unit investment cost of CFPP are also considerable, it should be recognized there is limited potential for investment reduction as the technology of CFPP is already mature. Conversely, the unit investment costs of the PCS part of BESS, as well as the charge and discharge parts of TESS, have negligible influence. The impacts of the unit investment cost of WT and coal price are exceedingly significant; a 10 % reduction in either can lead to an approximate 2.4 % decrease in LCOE. Future efforts could focus on reducing the values of these two parameters through technological advancements and location-specific strategies to effectively reduce LCOE.

## 5. Conclusion

This study puts forward and deeply analyzes an integrated power

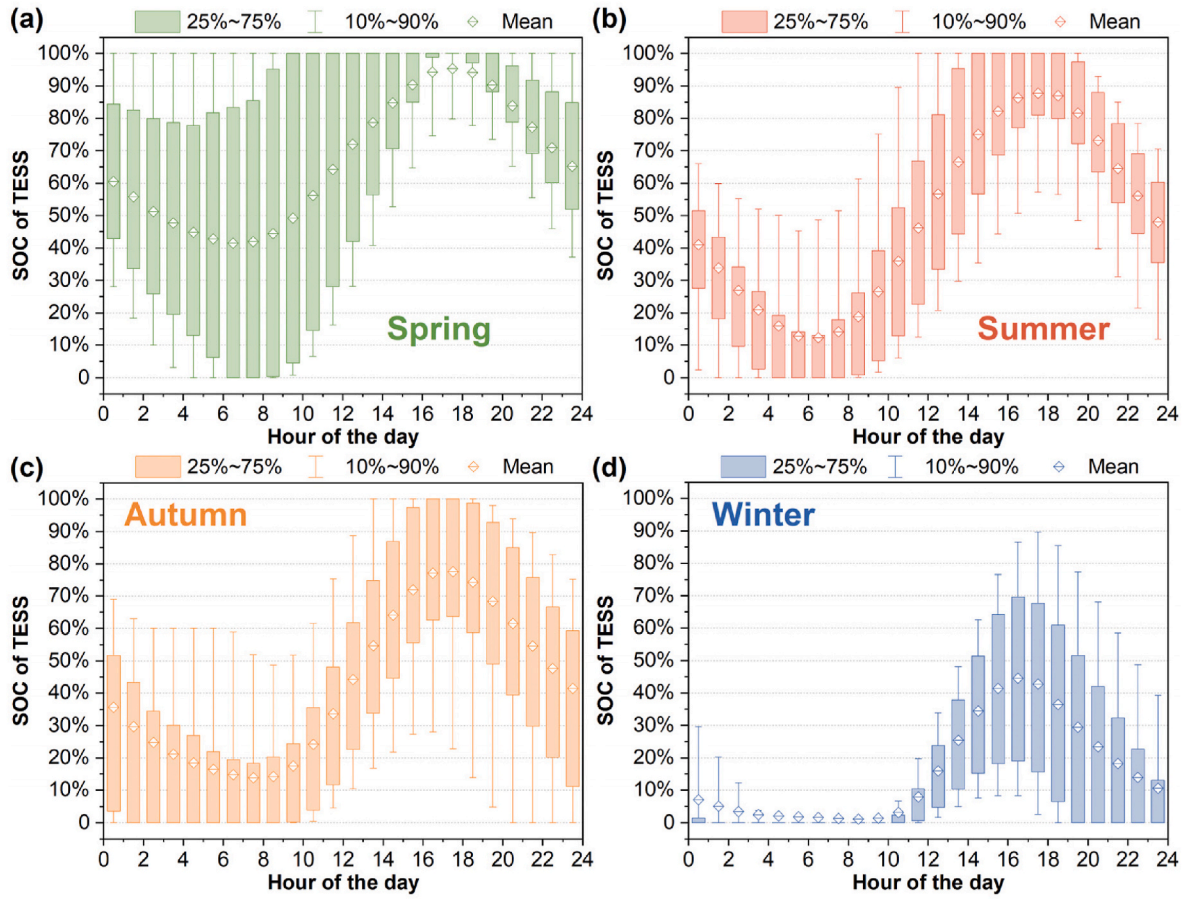


**Fig. 15.** Hourly distribution of SOC of TESS in different seasons.

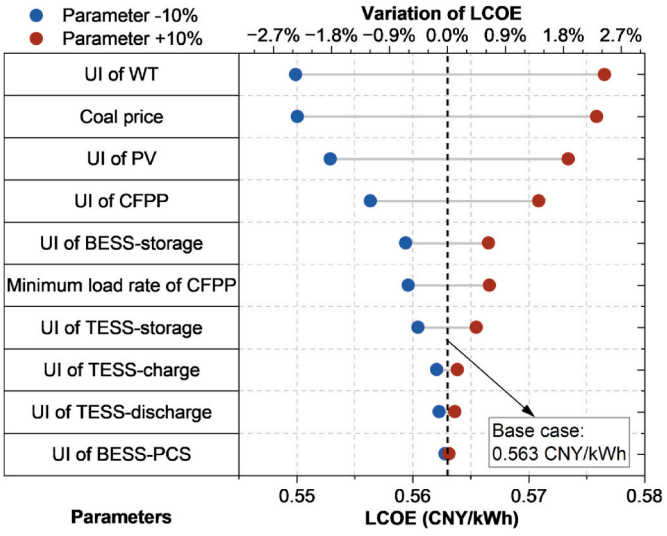


**Fig. 16.** Univariate sensitivity of LCOE to 10 % variations in technical and economic parameters.

system that combines CFPP with photovoltaic, wind power, and energy storage systems, which is suitable for areas with abundant wind and solar resources. Its operational characteristics are also analyzed deeply through operation simulation. The key insights presented in this paper are as follows.

(1) By integrating coal-fired power plant with photovoltaic power, wind power and energy storage, the specific $CO_2$ emission can reach the same level as NGCC, while the LCOE is lower. When the specific $CO_2$ emission is controlled at 349g/kWh (NGCC level), the LCOE of the optimal configuration stands at 0.563 CNY/kWh, representing a 12 % reduction compared to NGCC (0.643 CNY/kWh).

(2) The specific $CO_2$ emission has obvious seasonal characteristics and large intraday fluctuations. The specific $CO_2$ emission is the lowest in summer and from 10:00 to 18:00 in a day. The fluctuations in wind resources, solar resources, and power demand are the main reasons for the fluctuations in specific $CO_2$ emission.

(3) The CFPP operates in a mode of lower load during the daytime and higher load at night. Furthermore, the CFPP actively contributes to peak-shaving tasks, taking on a critical role in balancing the power demand, thereby enhancing the reliability and stability during periods of peak power consumption.

(4) The BESS plays a critical role in daily peak-shaving tasks. Its SOC exhibits predictable fluctuations, with a consistent pattern of higher levels in the afternoon and lower levels at night, which is good for the health of the battery pack and convenient for formulating maintenance plans. The TESS plays a role in dealing with the random fluctuations of VRE output and power demand, ensuring the reliability of the integrated system.

However, there are still several aspects that need to be improved. Although the proposed system has significant potential for providing peak-shaving services to the power grid, the extent of its peak-shaving capacity has not been thoroughly assessed. Furthermore, renewable energy curtailment is a prevalent issue during the spring and summer,

necessitating the exploration of demand-side management strategies to mitigate the extensive curtailment [67]. Conversely, in winter, high carbon emissions with significant variance are observed. It is imperative to integrate data-driven optimal power scheduling strategies such as power demand forecasting and renewable energy power output predictions, thereby adjusting the operational schedules of CFPP to reduce carbon emissions. These identified research limitations could serve as promising directions for future investigations.

## CRediT authorship contribution statement

**Yuhao Shao:** Writing – original draft, Visualization, Methodology, Data curation. **Tian Wu:** Writing – original draft, Data curation. **Xinrong Yan:** Resources. **Chao Yang:** Writing – review & editing, Validation. **Lijie Wang:** Writing – review & editing, Validation. **Wenxuan Guo:** Formal analysis, Data curation. **Yangshu Lin:** Formal analysis, Data curation. **Yurong Xie:** Resources. **Yi Ding:** Supervision, Funding acquisition. **Chenghang Zheng:** Project administration, Methodology, Funding acquisition. **Xiang Gao:** Funding acquisition, Conceptualization.

## Declaration of competing interest

The authors declare that they have no known competing financial interests or personal relationships that could have appeared to influence the work reported in this paper.

## Acknowledgments

This work was supported by the National Natural Science Foundation of China (42341208), the "Pioneer" and "Leading Goose" R&D Program of Zhejiang (2023C03008), Major Consulting and Research Project of Zhejiang Research Institute of China Engineering Science and Technology Development Strategy (2023ZL0003).

## Appendix A. Supplementary data

Supplementary data to this article can be found online at https://doi.org/10.1016/j.energy.2025.135949.

## Data availability

Data will be made available on request.

## References

[1] Paris agreement. Report of the conference of the parties to the United Nations framework convention on climate change (21st session, 2015: Paris) 2016;4:2.
[2] Zhang D, Huang X, Zhong J. A representative $CO_2$ emissions pathway for China toward carbon neutrality under the Paris Agreement's 2 °C target. Adv Clim Change Res 2023;14:941–51.
[3] Riahi K, Vuuren DPV, Kriegler E. The Shared Socioeconomic Pathways and their energy, land use, and greenhouse gas emissions implications: an overview. Glob Environ Change 2016;42.
[4] Bhattacharya S, Banerjee R, Ramadesigan V. Bending the emission curve – the role of renewables and nuclear power in achieving a net-zero power system in India. Renew Sustain Energy Rev 2024;189:113954.
[5] Sun X, Bao M, Ding Y. Modeling and evaluation of probabilistic carbon emission flow for power systems considering load and renewable energy uncertainties. ENERGY 2024;296:130768.
[6] Herc L, Pfeifer A, Duić N. Economic viability of flexibility options for smart energy systems with high penetration of renewable energy. ENERGY 2022;252:123739.
[7] Pan T, Ocloń P, He L. Operational optimisation of integrated solar combined cooling, heating, and power systems in buildings considering demand response and carbon trading. Energy Convers Manag 2024;315:118737.
[8] Haran S, Rao AB, Banerjee R. Life cycle energy-carbon-water footprint assessment of an existing coal power plant retrofitted with calcium looping (CaL) based CCS system. Int J Greenh Gas Control 2023;130:104015.
[9] Araújo ODQF, Boa Morte IB, Borges CLT. Beyond clean and affordable transition pathways: A review of issues and strategies to sustainable energy supply. Int J Electr Power Energy Syst 2024;155:109544.
[10] Sun L, Li J, Guo Z. Construction of energy coupling system with multi-energy complementary and clean low-carbon. Journal of China University of Petroleum (Edition of Natural Science) 2023;47:130–7 (in Chinese).
[11] Han X, Liu D, Li H. Dynamic characteristics and control method of the solar-coal energy complementary system. ENERGY 2024;299.
[12] Han Z, Bai Y, Wang J. Optimization of a 600 MW supercritical solar-coal hybrid power plant and $CO_2$ reduction analysis. J China Coal Soc 2015:524–31 (in Chinese).
[13] Deguenon L, Yamegueu D, Moussa kadri S. Overcoming the challenges of integrating variable renewable energy to the grid: A comprehensive review of electrochemical battery storage systems. J Power Sources 2023;580:233343.
[14] Thanapalan K, Constant E. Overview of energy storage technologies for excess renewable energy production. 24th world multi-Conference on Systemics, Cybernetics and Informatics, WMSCI 2020. September 13, 2020 - September 16, 2020, 2020.
[15] Zou Y, Wang Q, Hu B. Hierarchical evaluation framework for coupling effect enhancement of renewable energy and thermal power coupling generation system. Int J Electr Power Energy Syst 2023;146.
[16] Tahir MF, Haoyong C, Mehmood K. Integrated energy system modeling of China for 2020 by incorporating demand response, heat pump and thermal storage. IEEE Access 2019;7:40095–108.
[17] Liu T, Yang J, Yang Z. Techno-economic feasibility of solar power plants considering PV/CSP with electrical/thermal energy storage system. Energy Convers Manag 2022;255:115308.
[18] Yang J, Yang Z, Duan Y. Optimal capacity and operation strategy of a solar-wind hybrid renewable energy system. Energy Convers Manag 2021;244:114519.
[19] Li R, Guo S, Yang Y. Optimal sizing of wind/concentrated solar plant/electric heater hybrid renewable energy system based on two-stage stochastic programming. ENERGY 2020;209:118472.
[20] Li W, Zhang Z, Zhang X. Oilfield load flexible adjustment characteristics based optimal operation regulation strategy of multi-energy Complementary system. 2023.
[21] Smith RW. 4 - Steam turbine cycles and cycle design optimization: Combined cycle power plants. In: Tanuma T, editor. Advances in steam turbines for modern power plants. Woodhead Publishing; 2017. p. 57–92.
[22] Khallaghi N, Hanak DP, Manovic V. Techno-economic evaluation of near-zero $CO_2$ emission gas-fired power generation technologies: A review. J Nat Gas Sci Eng 2020;74:103095.
[23] Shao Y, He X, Yang C. Techno-economic evaluation of $CO_2$ capture and storage retrofit in decarbonizing different thermal power plants: A case study in China. Appl Therm Eng 2024;242:122380.
[24] Adams T, Mac Dowell N. Off-design point modelling of a 420MW CCGT power plant integrated with an amine-based post-combustion $CO_2$ capture and compression process. APPLIED ENERGY 2016;178:681–702.
[25] Carapellucci R, Giordano L. Upgrading existing gas-steam combined cycle power plants through steam injection and methane steam reforming. ENERGY 2019;173:229–43.
[26] Thallam Thattai A, Woudstra T, Wittebrood BJ. System design and exergetic evaluation of a flexible integrated reforming combined cycle (IRCC) power plant system with carbon dioxide ($CO_2$) capture and metal hydride based hydrogen storage. Int J Greenh Gas Control 2016;52:96–109.
[27] Rúa J, Nord LO. Optimal control of flexible natural gas combined cycles with stress monitoring: Linear vs nonlinear model predictive control. APPLIED ENERGY 2020;265:114820.
[28] Wang Y, Wang H, Razzaghi R. Multi-objective coordinated EV charging strategy in distribution networks using an improved augmented epsilon-constrained method. APPLIED ENERGY 2024;369:123547.
[29] Khan A, Javaid N. Jaya learning-based optimization for optimal sizing of stand-alone photovoltaic, wind turbine, and battery systems. Engineering 2020;6:812–26.
[30] Wang JL, Guo S, He Y. Multi stage planning and operation optimization of hybrid renewable energy systems with flexible hydrogen-battery storage. Acta Energiae Solaris Sin 2024;45:41–9 (in Chinese).
[31] Maleki A, Pourfayaz F. Optimal sizing of autonomous hybrid photovoltaic/wind/battery power system with LPSP technology by using evolutionary algorithms. Sol Energy 2015;115:471–83.
[32] Amrollahi MH, Bathaee SMT. Techno-economic optimization of hybrid photovoltaic/wind generation together with energy storage system in a stand-alone micro-grid subjected to demand response. APPLIED ENERGY 2017;202:66–77.
[33] Xu X, Hu W, Cao D. Optimized sizing of a standalone PV-wind-hydropower station with pumped-storage installation hybrid energy system. Renew Energy 2020;147:1418–31.
[34] Nirbheram JS, Mahesh A, Bhimaraju A. Techno-economic optimization of standalone photovoltaic-wind turbine-battery energy storage system hybrid energy system considering the degradation of the components. Renew Energy 2024;222:119918.
[35] National solar radiation database. https://nsrdb.nrel.gov/data-viewer. [Accessed 10 November 2023].
[36] Liu T, Yang Z, Duan Y. Techno-economic assessment of hydrogen integrated into electrical/thermal energy storage in PV+ Wind system devoting to high reliability. Energy Convers Manag 2022;268:116067.
[37] Han Q, Wang T, Chu F. Nonparametric copula modeling of wind speed-wind shear for the assessment of height-dependent wind energy in China. Renew Sustain Energy Rev 2022;161:112319.
[38] Gipe P. Wind energy comes of Age. John Wiley & Sons, Inc; 1995.

[39] Aldersey-Williams J, Rubert T. Levelised cost of energy – a theoretical justification and critical assessment. Energy Policy 2019;124:169–79.
[40] Chen H, Wang C, Ye M. An uncertainty analysis of subsidy for carbon capture and storage (CCS) retrofitting investment in China's coal power plants using a real-options approach. J Clean Prod 2016;137:200–12.
[41] Fan J, Wei S, Yang L. Comparison of the LCOE between coal-fired power plants with CCS and main low-carbon generation technologies: Evidence from China. ENERGY 2019;176:143–55.
[42] Yang L, Xu M, Fan J. Financing coal-fired power plant to demonstrate CCS (carbon capture and storage) through an innovative policy incentive in China. Energy Policy 2021;158:112562.
[43] China Electricity Council. Annual development Report of China's power Industry 2023, China Building materials. Beijing: Press; 2023 (in Chinese).
[44] Dong Y, Jiang X, Liang Z. Coal power flexibility, energy efficiency and pollutant emissions implications in China: A plant-level analysis based on case units. Resour Conserv Recycl 2018;134:184–95.
[45] Load profiles of national grid. https://www.nationalgridus.com/Upstate-NY-Business/Rates/Load-Profiles. [Accessed 10 November 2023].
[46] Zhang G, Shi Y, Maleki A. Optimal location and size of a grid-independent solar/hydrogen system for rural areas using an efficient heuristic approach. Renew Energy 2020;156:1203–14.
[47] Ma T, Javed MS. Integrated sizing of hybrid PV-wind-battery system for remote island considering the saturation of each renewable energy resource. Energy Convers Manag 2019;182:178–90.
[48] LONGi green energy technology Co., Ltd, Product specification of LR5-72HPH. https://www.longi.com/eu/download/?categoryId=296&productClassificationId=245. [Accessed 5 May 2024].
[49] Goldwind Sci & Tech Co. Ltd, Product specification of GW150-3.0MW. https://www.goldwind.com/en/windpower/product-gw2s/. [Accessed 15 June 2024].
[50] China Electric Power Planning & Engineering Institute. Thermal power engineering quota design reference cost index 2020 level. Beijing: China Electric Power Press; 2021 (in Chinese).
[51] China Electricity Council. Annual development Report of China's power Industry 2022, China Building materials. Beijing: Press; 2022 (in Chinese).
[52] Zhao C, Zhang W, Wang Y. The economics of coal power generation in China. Energy Policy 2017;105:1–9.
[53] Shao Y, He X, Yang C. Techno-economic evaluation of $CO_2$ capture and storage retrofit in decarbonizing different thermal power plants: a case study in China. Appl Therm Eng 2024;242:122380.
[54] Cao Y, Chen J, Liu B. China zero-carbon electricity growth in the 2020s: A vital step toward carbon neutrality. Energy Transitions Commission and Rocky Mountain Institute 2021.
[55] China Electricity Council. Study on flexible operation and life extension operation of coal-fired power units. Beijing. 2020 (in Chinese).
[56] Yin G, Duan M. Pricing the deep peak regulation service of coal-fired power plants to promote renewable energy integration. APPLIED ENERGY 2022;321:119391.
[57] Seto KC, Davis SJ, Mitchell RB. Carbon lock-in: Types, causes, and policy implications. Annu Rev Environ Resour 2016;41:425–52.
[58] Tong D, Zhang Q, Zheng Y. Committed emissions from existing energy infrastructure jeopardize 1.5 °C climate target. NATURE 2019;572:373–7.
[59] Coal database. https://www.cctd.com.cn/list-167-1.html. [Accessed 28 May 2022] [in Chinese)].
[60] Mo J, Cui L, Duan H. Quantifying the implied risk for newly-built coal plant to become stranded asset by carbon pricing. Energy Econ 2021;99:105286.
[61] Shan Y, Guan D, Zheng H. China $CO_2$ emission accounts 1997–2015, vol. 5. Scientific Data; 2018.
[62] Liu J. Economic assessment for energy storage technologies adaptive to variable renewable energy. Energy Storage Science and Technology 2022;11:397–404 (in Chinese).
[63] China Renewable Energy Engineering Institute. China renewable energy development Report 2021. Beijing: China Water&Power Press; 2022 (in Chinese).
[64] Viswanathan V, Mongird K, Franks R. Grid energy storage technology cost and performance assessment. 2022.
[65] Ding Z, Hou H, Yu G. Performance analysis of a wind-solar hybrid power generation system. Energy Convers Manag 2019;181:223–34.
[66] Wang Y, Qiu J, Tao Y. Optimal power scheduling using data-driven carbon emission flow modelling for carbon intensity control. IEEE Trans Power Syst 2022;37:2894–905.
[67] Sousa J, Soares I. Benefits and barriers concerning demand response stakeholder value chain: a systematic literature review. ENERGY 2023;280:128065.